공학박사 학위논문

Mechanically Stable Hydroxyapatite Patterning with Biological Functions for Tissue Regeneration

다양한 생체 기능과 기계적 안정성을 갖는 하이드록시아파타이트의 조직 재생용 패터닝

2021년 2월

서울대학교 대학원

재료공학부

강 인 구

Mechanically Stable Hydroxyapatite Patterning with Biological Functions for Tissue Regeneration

다양한 생체 기능과 기계적 안정성을 갖는
하이드록시아파타이트의 조직 재생용 패터닝

지도교수 김 현 이

이 논문을 공학박사 학위논문으로 제출함

2021년 2월

서울대학교 대학원
재료공학부
강 인 구

강 인구의 박사 학위논문을 인준함

2020년 12월

위 원 장 안 철 희 (인)
부위원장 김 현 이 (인)
위 원 남 기 태 (인)
위 원 한 철 민 (인)
위 원 정 현 도 (인)

Abstract

Mechanically Stable Hydroxyapatite Patterning with Biological Functions for Tissue Regeneration

In-Gu Kang
Department of Materials Science and Engineering
Seoul National University

Hydroxyapatite (HA), a component of human bone tissue, is a promising material which is widely accepted in tissue regenerating applications. In many cases, HA is coated on metal implant surface to enhance biocompatibility for tissue fixation. However, due to its inherent brittleness, HA is hard to be applied on metal implants with complex shape or flexible polymer surface. Here, micro-patterning can be an alternative for surface application of brittle HA. HA micro-pattern fabricated by photolithography was introduced on polymer surface by our novel transferring technique. With this method, brittle HA can be applied on the flexible bio-polymer surface with mechanical stability,

imparting enhanced biocompatibility.

In the first study, we fabricated a linear HA pattern on a silicon wafer and then transferred the pattern to a poly(L-lactic)-acid (PLLA) film for use as a tubular vascular graft. The bioactive HA pattern can impart biocompatibility on the bio-inert polymeric vascular graft. The HA pattern with its characteristic needle-like shape was successfully embedded into the PLLA. The HA-patterned PLLA film exhibited superior mechanical stability compared with that of a HA-coated PLLA film under bending, elongation, and *in vitro* circulation conditions, suggesting its suitability for use as a tubular vascular graft. In addition, the HA pattern guided rapid endothelialization by promoting proliferation of endothelial cells and their migration along the pattern. The hemocompatibility of the HA-patterned PLLA was also confirmed, with substantially fewer platelets adhered on its surface. Overall, in addition to good mechanical stability, the HA-patterned PLLA exhibited enhanced biocompatibility and hemocompatibility compared with pure PLLA.

In the second study, we developed a noble method to pattern HA loaded with recombinant human bone morphogenetic protein-2 (rhBMP-2) on PLLA for GBR membrane. Successfully fabricated HA pattern was transferred to PLLA membrane with fixed and sound morphology in spite of mechanical stimuli. Protein was obviously attached on and under HA patterns contrary to

PLLA and released gradually from under-HA in the long term of 7 days. The amount of loaded rhBMP-2 was overwhelmingly large on under HA sample (u/HAP), attributed to the large surface area of hemispherical HA pattern. Cellular morphology and proliferation results supported the biological effect of HA on PLLA membrane. Osteoblastic differentiation results proved the large amount of rhBMP-2 from u/HAP, representing remarkable increase in ALP activity after 14 days of culturing. Animal experiments demonstrated the prolonged bone healing effect with releasing larger amount of rhBMP-2 under the HA pattern.

In conclusion, bioactive HA pattern was fabricated and transferred on PLLA surface, successfully imposing biocompatibility and additional drug loading capability. With this unique patterning and transferring technique, brittle biomaterials are expected to be applied on flexible polymer membrane, which can be employed in various tissue engineering applications.

Keywords: Hydroxyapatite; Poly(L-lactic)-acid; Micro-patterning; Transferring; Vascular graft; Endothelialization; Guided bone regeneration membrane; Bone regeneration; Recombinant human bone morphogenetic protein-2; Drug delivery;

Student number: 2015-20875

Contents

List of figures

wafer, and HA- patterned PLLA (★:Hydroxyapatite ●:Magnesium).

Figure 2.5. FE-SEM images of HA-coated and HA-patterned PLLA film before A), C) and after rolled up in tubular shape B, D).

Figure 2.6. A) HA-coated and B) patterned PLLA after 5% elongation. Insets show high magnification images of each surface C) HA-coated and D) patterned PLLA after 4 weeks of *in vitro* circulation in DBPS medium.

Figure 2.7. Representative CLSM images of HUVECs cultured on A) pure PLLA and B) HA-patterned PLLA after 24 hr.

Figure 2.8. Levels of cell viability on pure and HA-patterned PLLA after 2 and 5 days (*$p < 0.05$).

Figure 2.9. Representative CLSM images of HUVEC migration on A) pure and B) HA-patterned PLLA 24 hr after removing cell barrier (yellow arrow: migration direction, yellow dashed line: migration starting line).

Figure 2.10. Representative FE-SEM images of platelets attached on A) pure and B) HA-patterned PLLA, and C) the number of platelets counted per area (yellow arrow: platelets, *$p < 0.05$).

Figure 3.1. Scheme of A) HA and drug patterning on the PLLA film by photolithography and B) control groups.

Figure 3.9. Percentage of bone coverage on each sample six weeks after implantation based on the histological images (stained with Masson's Trichrome, $n = 3$, $*p < 0.05$).

Chapter 1.

Introduction

(Theoretical review)

1.1. Composite biomaterials for tissue regeneration

Increasing life expectancy and health concerns, tissue engineering which regenerates damaged tissue caused by injury or disease is extensively drawing attention. Tissue engineering is a process to replace or accelerate the regeneration of damaged or disordered tissue in human body [1-5]. The key factors for the process are scaffold, cells, and grow factors. Among these factors, the scaffold is crucial for playing a role as a mechanical supporter for surrounding tissue and providing the favorable room for the sufficient growth of cells. Hence, for cell growth and regeneration of tissue, the scaffold should be biocompatible [6-8]. Therefore, the scaffold needs to be mechanically sustainable and offer cell-friendly environment for tissue regeneration.

Polymer-based scaffold is attracting attention for both hard and soft tissue engineering due to its moderate mechanical properties and flexibility [9-11]. Among many kinds of biopolymers, poly(L-lactic)-acid (PLLA) has moderate biocompatibility and high mechanical modulus for retaining original shape. Also, PLLA is a biodegradable polymer, showing that polymer scaffold can be eroded and substituted with recovered tissue. However, PLLA is lack of biocompatibility to firmly attach to surrounding tissue or sufficiently induce tissue regeneration, possibly resulting in the failure of scaffold or immunological inflammation [12, 13]. To compensate the limitation of polymer

scaffold, biocompatible materials are commonly mixed in polymer matrix, making composite biomaterials.

Ceramic hydroxyapatite(HA) is one of the widely used materials for enhancing the biocompatibility of polymer matrix due to its great bioactivity. Because of its excellent biocompatibility, HA can be applied on both hard and soft tissue engineering [14, 15]. Being one of the components of human bone tissue, HA is known as osseoconductive material, which conduce the formation of new bone. In addition, HA is utilized on soft tissue regeneration due to its cell-friendly property. Generally, HA is simply mixed with polymer matrix to make the scaffold biocompatible in many researches [16, 17]. However, simply mixing method has a limitation that the composite hardly exposes the bioactive HA on its surface with a low fraction of HA. To make matters worse, increasing the fraction of HA can make the composite body brittle due to the brittle characteristic of ceramic HA [18]. So the mechanical properties of the composite are disrupted to be used as a scaffold.

In other method, ceramic HA can be coated on the scaffold surface, which is easily broken and delaminated from the surface owing to the brittleness of HA. Especially for polymer composites, the HA-coated layer is expected to be easily cracked and delaminated from the surface of polymer while winding the scaffold to apply on various implantation sites. It is attributed to the low binding affinity between HA and polymer and also the brittleness of

HA. And also, these coating fragments can be detrimental to surrounding tissue, which can lead to the foreign body reaction and inflammation. Synthetically, existing HA-polymer composite system has its drawback for maintaining the original mechanical properties of polymer.

1.2. Hydroxyapatite (HA) micro-patterning

Considering the drawbacks of conventional HA-polymer composite materials, simple mixing is not appropriate for the effective tissue regenerating applications. Therefore, another noble method for fabricating the composite introducing photolithography-based micro-patterning technique was tried in this research.

Micro-patterning with photolithography is of widespread use in semiconductor engineering, making it easy to generate micro-sized pattern precisely. Furthermore, photolithography technique is applied on various tissue engineering; from soft tissue to hard tissue regeneration [19-21]. However, the existing method is focused on generating micro- or nano-sized pattern and researching cellular reaction on the pattern in usual, which is not yet in a practical stage.

In this research, we are focused on making HA-polymer composite

using micro-patterning technique. Fabricated with photolithography, HA pattern can be transferred on the polymer surface. Different from the usual simply-mixed-composite, our system introduces HA micro-pattern onto the polymer surface. So HA micro-patterns are exposed on the polymer scaffold surface and making it cell-friendly, improving the initial cell attachment and proliferation. Thanks to its morphological difference from the original composites, this system is not detrimental for the mechanical properties of polymer matrix.

Besides, the morphology of HA pattern is embedded structure, making it mechanically stable structure. The stability of pattern is beneficial for maintaining biocompatibility on polymer for longer term and applying on curved or irregular surface. The embedded pattern would not easily be detached from the polymer surface thanks to the morphological characteristic of HA crystal, though the matrix is curved or stretched on the various implantation sites. So the patterned structure is expected to retain its morphology on the complexly-shaped implant sites.

1.3. Biological functions

Based on our noble ceramic HA micro-patterning and transferring

method, we could obtain the unique HA-polymer bio-composite. However, we can also expect other additional biological functions using the specific shape and characteristics of HA pattern itself and the bio-affinity of HA with biomolecules.

1.3.1. Biological functions depending on pattern shape

Among all biological functions, imposing bioactivity on the polymer scaffold is the most important property. As mentioned in a previous part, HA is a highly bioactive material, which is considerably attracting various kinds of cells to attach and proliferate on its surface. Making the most of this cell-friendly and –attracting property, we can stimulate the cellular reaction on the implant surface.

In the first study, linear type HA pattern was adopted on PLLA membrane for vascular regenerating application. In many researches, HA is also known to improve the initial attachment and proliferation of vascular endothelial cells, and the process is known as endothelialization [22, 23]. Additionally, the shape of pattern (linear) was chosen to boost the speed of endothelial cell migration and cell recovery, providing cell-friendly “road” on the graft surface. In many researches, topographical linear pattern was effective

in stimulating endothelialization [23]. Linear patterns with diverse width were dealt with from nano-size to mico-size in vascular graft applications. Similar with previous researches, cell-favorable linear HA pattern can also control the direction of cell growth and migrating speed. In addition, because cells tend to attach and elongate along the linear pattern, the attached morphology would mimic that of the original shape of blood vessel(Fig.1.1), which shows the elongated and aligned endothelial cells on the vessel wall [24]. Therefore, the HA pattern not merely enhances biocompatibility of the scaffold but also performs a biological function for endothelialization.

In the second study, round type HA pattern was utilized instead of linear one. Round type pattern was applied on PLLA-based guided bone regeneration(GBR) membrane, which is quite more dramatically bent or stretched on the affected bone area(Fig.1.2). Also, during fixing the membrane, stress is more frequently applied on itself. So the round type pattern would be much more stable rather than the linear type in every loading direction on the GBR membrane. Consequently, mechanically stable HA-patterned GBR membrane can retain the bioactivity of its surface, offering better environment in longer term of bone tissue regeneration.

1.3.2. High-dose drug loading reservoir

In another point of view, HA pattern can be utilized in drug delivery system. In many researches, the micro-pattern on the surface of membrane-type implant was employed as a drug loading site [25]. It has an advantage that can control the release of drug and make a room for drug loading inside the drug-repelling polymer.

Typically, polymers have much less number of surface functional groups than HA, making them hard to bind with biomolecules. But many researches tried to load biomolecules in polymer scaffold with various structures though they were not effective to load sufficient amount for tissue recovery [26, 27].

On the contrary, crystallized HA has a morphology of highly needle-like structure, providing a sufficient niche for biomolecule loading. Additionally, HA is represented to have a good affinity with biomolecules based on the electrostatic and hydrogen bonding [28]. Therefore, with the same surface area, HA with higher biomolecular affinity binds and loads a larger amount of biomolecule on its surface than polymer materials do. Consequently, our noble transferrable HA pattern is anticipated to be used as a high-dose drug reservoir despite the low drug affinity of the polymer membrane.

1.4. Aim of the studies

The aim of this study is imposing biocompatibility on polymer implants with bioactive HA micro-patterning and applying additional biological functions for different medical applications. Although polymer membranes are utilized in orthopedic and dental applications, still many issues are emerged in their low biocompatibility. Also, for the effective regeneration of damaged tissue, additional functions are required. For accomplishing this assignment, different strategies for different medical devices were designed.

In the first study, PLLA membrane, which is commonly adopted in vascular graft application, was modified with bioactive HA micro patterns on its surface. Different from the common HA coating methods, micro-pattern-based surface modification is mechanically more stable with enhancing biocompatibility. In addition, linear HA pattern is anticipated to promote the endothelialization by stimulating the endothelial cell migration for vascular graft application.

In the second study, HA micro patterns were applied on GBR application for osseoconductivity and biomolecule delivery, working as a reservoir. HA is known to conduce the regeneration of bone and make GBR membrane contact tightly with surrounding tissue, presenting the membrane

failure. Moreover, HA performing a great interaction with biomolecules is expected to play as a drug loading site with a larger amount and controlled release.

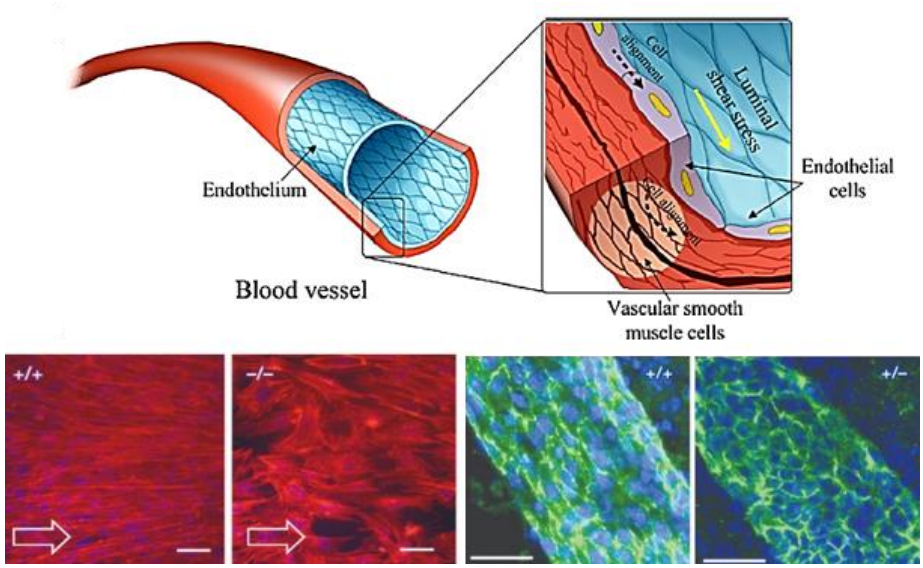

Figure 1.1. Graphical image of the intimal cellular structure of blood vessel with aligned vascular endothelial cell layer(endothelium) and its mimicking experiment with the elongated cells aligning along the linear pattern matrix.

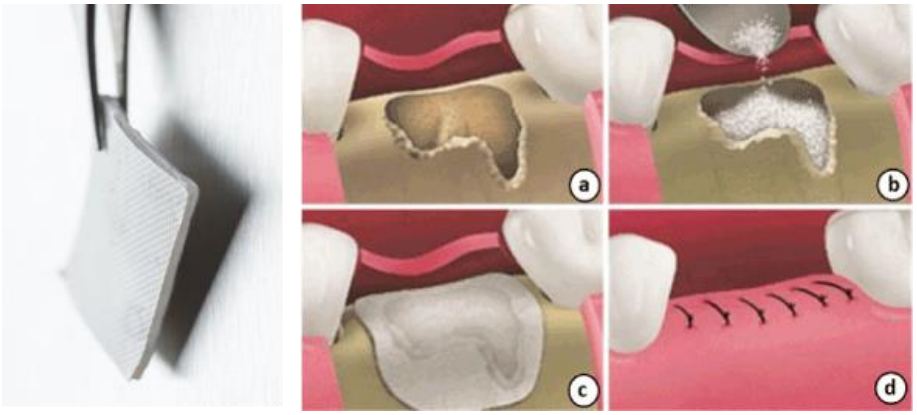

Figure 1.2. Graphical image of GBR membrane applied for dental implant application.

Chapter 2.

Embedded HA micro-pattern for vascular tissue regeneration

2.1. Introduction

Cardiovascular diseases, covering a damage or clogging of coronary arteries, require urgent replacement of the blood vessels [29-34]. Vascular grafts made of synthetic polymers, including expanded polytetrafluoroethylene (ePTFE) and Dacron (poly(ethylene terephthalate) are suitable candidates for replacing these injured vessels because of excellent mechanical properties [35-37]. Nowadays, biocompatible and biodegradable polymers, such as polycaprolactone (PCL), poly(lactic-co-glycolic acid) (PLGA), and PLLA have also been widely applied for vascular applications [38-41]. However, synthetic polymers encounter limitations for adoption as small-diameter grafts because they are easily clogged owing to their high thrombogenic property and poor degradability [12, 13, 42]. Biodegradable polymers have demonstrated superior biocompatibility than synthetic polymers and do not require secondary surgery for removal. Even though biodegradable polymers have shown advanced functionality, particularly for small-diameter grafts, they still lack of bioactivity, which commonly result in delayed endothelialization on the intimal surface of vascular grafts [43, 44].

Patterning of bioactive material on implants is a promising technique because of the ability to achieve mechanical stability for complex shapes. Micro-patterns exhibit superior mechanical stability compared with

conventional ceramic coatings because stress can be distributed through the very ductile polymeric phase. In addition, a bioactive linear micro-pattern can guide cellular migration. The guidance of cellular migration leads to faster recovery of tissue, which can be beneficial for vascular grafts or other bio-implant applications [45-48].

HA is a well-known bio-ceramic that is generally used in hard tissue engineering. Recent studies have verified the usefulness of HA in soft tissue regeneration [49, 50]. Its high bioactivity can be beneficial for polymer-based vascular grafts by enabling the adsorption of cell adhesion proteins on the surface, which leads to rapid endothelialization [50-53]. However, the brittleness of HA poses an intrinsic limitation for its application in polymer vascular grafts and can be improved by patterning.

In this study, a linear HA pattern was introduced on a PLLA biopolymer vascular graft using a unique pattern transferring technique [54]. Photolithography was performed to fabricate the linear HA pattern on a silicon (Si) wafer, which was then transferred to a PLLA film. The stability of the HA pattern on the vascular graft was examined using mechanical bending, elongation, and *in vitro* circulation tests. *In vitro* cell and platelet tests revealed the improved biocompatibility and hemocompatibility of the film, respectively.

2.2. Experimental procedure

2.2.1. HA-Patterned Vascular Graft Fabrication

2.2.1.1. HA patterning

A linear HA pattern was fabricated using a typical photolithography technique [54]. First, a 1.5-μm-thick photoresist (AZ 5214E, Microchemicals, Germany) was uniformly coated on the Si wafer by spin coating. A mask aligner (Karl-Suss MA-6, Suss MicroTec, Germany) was used to make a specific pattern (20-μm width and 50-μm gap) by exposing the photoresist film to ultraviolet (UV) light through the precisely designed photomask. After the exposure, the UV-treated photoresist part was dissolved using a developer solution (AZ 300 MIF, Microchemicals, Germany), and a linear photoresist pattern with a width of 50 μm and gap of 20 μm was obtained. On this patterned photoresist, a 1-μm-thick pure Mg layer was deposited using an electron-beam evaporation system (EVACO-EB800R, DR Vacuum Inc., Korea). The Mg-deposited sample was immersed in acetone to wash away the remaining photoresist, and then, a linear Mg pattern with a 20-μm width and 50-μm gap was obtained on the Si wafer. This linear Mg pattern was then converted into HA using a previously described method [54]. Briefly, the Mg-patterned Si was immersed in a 0.05 M ethylenediaminetetraacetic acid calcium disodium salt hydrate (Ca-EDTA, Sigma Aldrich, USA)/0.05 M potassium dihydrogen

phosphate (KH_2PO_4, Sigma Aldrich, USA) aqueous solution at 90℃ and pH 8.9 for 2 h.

2.2.1.2. HA Pattern Transfer

The as-prepared HA pattern on the Si wafer was transferred to a polymer film using a simple solvent casting method. First, a solution of 10 wt% PLLA (99.9%, M_n = 60,000–80,000, Pureco Co., Korea) in dichloromethane (DCM, Sigma Aldrich, USA) was poured onto the HA-patterned Si wafer. After evaporation of DCM, the PLLA film with HA pattern was peeled off from the Si wafer surface. The brief fabrication process of the vascular graft is illustrated in Fig.2.1. The process consisted of two steps: HA patterning and transfer (Fig.2.1). Additionally, a HA layer was fabricated on a Si wafer without patterning and then transferred onto the PLLA surface to verify the stability of the linearly patterned HA.

2.2.2. Characterization of HA Pattern

The surface morphology of the HA pattern and patterned PLLA film were examined using field-emission scanning electron microscopy (FE-SEM; MERLIN Compact, ZEISS, Germany) and energy-dispersive X-ray spectrometry (EDS; X-maxN, Oxford Instruments, UK) mapping. The HA

pattern and patterned PLLA film were sectioned using focused ion beam milling (FIB, AURIGA, Zeiss, Germany), and cross-sectional images were acquired using FE-SEM coupled with FIB. The crystalline phases of each specimen were characterized using X-ray diffraction (XRD; D8-Advance, Bruker, Germany).

2.2.3. Stability Testing

The stability of the HA pattern on the PLLA film as a vascular graft was evaluated using bending, elongation, and *in vitro* circulation tests. To verify the superiority of the HA pattern, a HA-coated PLLA without patterning was also fabricated. The HA-patterned and HA-coated PLLA films were rolled up to form a tubular shape similar to a blood vessel. The vascular tube was rolled around a stainless steel rod with 3 mm in diameter and 20 mm in length. After rolled, DCM was applied on the edge parts and attached for the fixation. Specifically, the patterned film was rolled up with the patterns lying along their axis direction.

For the elongation tests, rectangular specimens with dimensions of 10 mm × 40 mm were used. The patterned film was elongated in the transverse direction using a tensile testing instrument (Model 5565, Instron Corp., USA) with up to 5% strain. After the sample was elongated, they were examined using

FE-SEM to observe any mechanical damage on the HA pattern or coating layer. In addition, circulation tests were performed using a perfusion pump (SciQ 323, Watson Marlow, UK). The circulating medium was Dulbecco's phosphate-buffered saline (DPBS, Welgene, Korea), and the flow rate was approximately 90 mL/min to mimic the human blood circulation system [55]. The medium was changed every 2 days, and after 4 weeks, the grafts were sectioned, unrolled, and evaluated using FE-SEM.

2.2.4. *In vitro* studies

The effect of the HA pattern on the cellular behavior was evaluated in terms of in vitro cell morphology, migration, and proliferation. The HA-patterned and pure PLLA were sterilized by immersion in 70% ethanol for 1 h and UV irradiation for 24 h. Human umbilical vein endothelial cells (HUVECs) were seeded on each sample with a density of 5×10^4 cells/mLand cultured in an endothelial cell basal medium-2 (EBM-2; Lonza, USA) with 10% fetal bovine serum (Life Technologies, Inc., USA) and 1% antibiotics (100 U/mL of penicillin and 100 μg/mL of streptomycin, GIBCO, USA) in a humidified incubator with 5% CO_2 at 37℃. After 1 day of culturing, the cells were fixed in 4% paraformaldehyde for 10 min, rinsed 3 times with DPBS, and treated with 0.1% Triton X-100 for 5 min and 1% bovine serum albumin (BSA) for 30

min. The cells were then stained with fluorescent Alexa Fluor 546 phalloidin (Molecular Probes, Eugene, USA) for 20 min and 4′,6-diamidino-2-phenylindole (Molecular Probes, Eugene, USA) for 5 min. Then, the morphology was examined using confocal laser scanning microscopy (CLSM; SP8 X, Leica, Germany).

The proliferation rate of the HUVECs was determined using the methoxyphenyl tetrazolium salt (MTS) assay (CellTiter 96 Aqueous One Solution, Promega, USA) after 2 and 5 days of culturing (n = 4). The amount of formazan, proportionate to the number of living cells, was checked by monitoring the light absorbance at a wavelength of 490 nm with a micro-reader (EZ Read 400, Biochrom, UK).

Finally, the effect of the HA patterning on promoting the migration of endothelial cells was evaluated. First, a titanium (Ti) cell barrier block was placed on the upper half of each film to interrupt the cell migration, and the HUVECs were cultured on the unblocked area for 3 days. After the HUVECs fully covered the unblocked area, the Ti block was removed and further incubated for 24 h to allow the HUVECs to migrate before observation using CLSM.

2.2.5. Platelet adhesion test

The hemocompatibility of the vascular grafts was assessed using platelet adhesion tests. Platelet-rich plasma (KOREAN Redcross Blood Services, Korea) was used for the experiment and diluted with DPBS at a 1:10 ratio. The suspension was spread on both the pure and patterned PLLA films, which were then incubated at 37℃ for 1 h. After rinsing with DPBS, the samples were fixed with 2.5 % glutaraldehyde solution for 1 h. The samples were then dehydrated using a gradient step with ethanol solutions (50%, 60%, 70%, 80%, 90%, 95%, and 100%), each for 10 min. After fixation and dehydration, the samples were observed using FE-SEM, and the number of platelets on the surface was counted (n = 5).

2.2.6. Statistical analysis

The statistical analysis was performed using statistical software (IBM SPSS statistics 23, IBM, USA). The data are shown as the mean ± standard error deviation. Statistical analysis was performed using a one-way analysis of variance (ANOVA), and p values less than 0.05 were considered statistically significant.

2.3. Results and discussion

2.3.1. Pattern on Si wafer

The synthesized HA pattern on the Si wafer was characterized using FE-SEM and EDS mapping, as shown in Fig.2.2a. The linear pattern fabricated on the Si wafer was clearly observed in the secondary electron image. In the EDS mapping image, Ca (red) and P (yellow) signals and a Si (cyan) signal were detected on the ridge and groove of the pattern, respectively, suggesting that the Mg pattern was successfully converted to calcium phosphate (CaP). During the conversion of Mg to HA, hydroxyl ions were generated from the ionization of Mg, which reacted with Ca and P ions, forming hydroxyapatite [56]. The morphology of the linear pattern was also examined at high magnification (Fig.2.2b). On the linear pattern, a distinguishing porous structure was observed.

The cross-section of the linear pattern was examined for further inspection of the morphology of linear pattern, as shown in Fig.2.2c. The individual ridge was round with dimensions of approximately 30–40 μm in width and 5 μm in height; these dimensions were originally 20 μm in width and 1 μm in height before the conversion. This change in the ridge dimensions also supports the suggested mechanism of Mg to HA conversion. In addition, no cracks or damaged parts were observed inside the linear pattern.

2.3.2. Pattern-transferred PLLA

After identifying the linear CaP pattern on the Si wafer, pattern-transferred PLLA was also characterized using similar methods. For the CaP-patterned PLLA, the C signal (blue) was detected between the linear CaP patterns (red and yellow), instead of Si, as shown in Fig.2.3a. This EDS mapping result confirms that the CaP pattern was successfully transferred to the PLLA matrix. The FIB-milled cross-sectional image is presented in Fig.2.3b. The needle-like CaP phase clearly formed tight interlocking with the PLLA matrix without any notable pores at the interface. Because there was no chemical bonding between the CaP and PLLA phases, this tight interlocking would contribute to the mechanical stability between the two phases under external loading.

2.3.3. Characterization of crystalline phases

The crystalline phases of the linear patterns on the Si wafer before and after conversion and of the pattern-transferred PLLA film were characterized using XRD. The XRD pattern of Mg (Fig.2.4) contained peaks at 33° and 34.5°. After the conversion, specific peaks of the crystalline HA phase were detected at 26°, 31.8°, 32.1°, and 34°, indicating that the Mg pattern was successfully

converted into a HA pattern. Additionally, these sharp peaks indicate the high crystallinity of the synthesized HA phase, which is important for biological properties of biomaterials [57-59]. Identical HA peaks were maintained after transfer to the PLLA matrix. For the peaks at 31°–35°, an increase in intensity was observed, which originated from the overlap between the peaks of the HA phase and the broad peak of the PLLA phase [60].

2.3.4. Stability of HA-patterned PLLA

The stability of the patterned HA on the PLLA film was compared with a HA layer coated on PLLA without patterning using several testing methods. First, the stability was evaluated by applying mechanical loading, namely rolling up and elongating the film. Fig.2.5 presents FE-SEM images of the HA pattern and HA coating layer before and after rolling up. As observed in Fig. 5a, the HA-coated film had a clear surface without any cracks directly after fabrication, although some large debris was detected on the surface. However, when the film was rolled up into a tubular shape (Fig.2.5b), numerous cracks were generated at the surface (yellow arrows). The cracked HA layer could be easily delaminated from the PLLA surface or fracture into debris, which could cause damage to blood vessels or foreign body reactions. The stability of the HA phase is thus important in vascular applications to prevent possible late-

stage graft occlusions [61]. Less debris was observed on the HA-patterned film than on the HA-coated PLLA before rolling up, as shown in Fig.2.5c. After rolling up, a few cracks were observed at the interface between HA and PLLA; however, no delamination or severe cracks were detected on the HA (Fig.2.5d), demonstrating the stability of the HA pattern.

The rolling-up method generates limited strain on the films depending on the curvature. Elongation tests were thus performed to apply much larger strain on the HA phases. Because of the larger strain, the HA coating layer on the PLLA film exhibited severe cracking (Fig.2.6a). Compared with the rolling-up test, larger cracks were also detected at the interface between HA and PLLA on the HA-patterned PLLA. However, no noticeable cracks were detected on the HA pattern itself (Fig.2.6b).

Finally, *in vitro* circulation tests were performed to simulate the real-life situation in blood vessels. A dramatic change was observed on the surface of the HA-coated sample. Most of the HA coating layer delaminated from the surface after 4 weeks of circulation, and only some HA flakes unstably dangled on the surface (Fig.2.6c). However, the HA pattern was still embedded inside the PLLA matrix, and detachment was not observed across the entire surface after the 4-week circulation period (Fig.2.6d). These results provide strong evidence of the flexibility of the patterned HA on the membrane, which could

be an advantage for application on curved parts of the human body [62].

2.3.5. *In vitro* endothelialization on HA-patterned PLLA

The effects of the linear HA pattern on the *in vitro* endothelial cell behaviors, namely, adhesion, proliferation, and migration, were examined. The morphology of the HUVECs was monitored using CLSM after 24 h of incubation (Fig.2.7). The HUVECs hardly attached on the pure PLLA surface (Fig.2.7a). In biological conditions, the hydrophobic surface of PLLA is difficult to coat with biomolecules, leading to less adhesion of cells [63]. In addition, the attached HUVECs exhibited a low level of activation. The cytoplasm of the HUVECs did not spread actively and had a round and dwindle-shaped morphology on the PLLA surface. More cells adhered on the HA-patterned PLLA surface with actively spread morphologies than on the pure PLLA surface (Fig.2.7b). Endothelialization, the formation of the endothelial cell layer on an intimal wall, is especially important in vascular applications [46, 64-66]. Therefore, imposing bioactivity to a PLLA matrix by HA patterning can be an advantage for vascular grafts. The adhered cells stretched along the direction of the HA patterns, demonstrating the compatibility of HA on endothelial cells.

The degree of cell proliferation was measured by the MTS assay

(Fig.2.8). After 2 days of culturing, the difference in the cell viability between pure and HA-patterned PLLA was not significant. The experimental period was considered to be too short to display a conspicuous gap. After 5 days, the proliferation level was significantly higher on the HA-patterned PLLA than on the pure PLLA group ($p < 0.05$). This improved cell proliferation can also be explained by the excellent ability of HA to proliferate endothelial cells [67, 68]. The compatibility of HA on endothelial cells has already been proven in other studies using attachment, proliferation, and animal tests [50, 67, 68]. This enhanced and faster proliferation of endothelial cells on HA-patterned PLLA suggests that faster endothelialization is possible in vascular applications [69-71].

The rapid endothelialization on the HA-patterned PLLA was further examined using migration tests. The migration rate is critical factor for the success of endothelialization on a vascular graft because endothelial cells should be recruited from adjacent blood vessels [46]. After removing the Ti block, cells migrated through the interface, indicated by the yellow dashed line in Fig.2.9. On the pure PLLA, the cells hardly migrated to the barred area, indicating the low endothelialization rate on pure PLLA (Fig.2.9a). The low rate of endothelialization could cause late vascular tissue regeneration and thrombogenesis [72-74]. However, more cells migrated into the blocked area

on the HA-patterned PLLA (Fig.2.9b). Furthermore, the majority of the migrated cells on the surface also elongated along the HA pattern. This finding suggests that the bioactive HA linear pattern would guide cells along the axis of the vascular tube, resulting in accelerated endothelialization on intima of artificial vascular grafts and rapid vascular tissue regeneration [46].

2.3.6. Platelet adhesion tests

To assess the hemocompatibility of the HA-patterned PLLA, platelet adhesion tests were performed. The morphologies of the adhered platelets on the pure and HA-patterned PLLA were observed using FE-SEM, as shown in Fig.2.10a and 2.10b, respectively. On the pure PLLA (Fig.2.10a), the platelets had a widely spread shape, which indicates their activated status. An activated platelet is considered one of the major causes of thrombogenesis and deterioration of the patency of a vascular graft [75]. In contrast, on the HA-patterned PLLA, platelets only adhered on the PLLA part (yellow arrows) and exhibited a dwindled morphology on the HA part (Fig.2.10b). The dwindled morphology of the platelets represents their resting stage. This morphological difference between PLLA and HA resulted from the foreign body reaction triggered by the hydrophobic surface of PLLA [76]. Hydrophobic surface has a

difficulty in absorbing proteins, resulting in platelet activation. Otherwise, hydrophilic surface like hydroxyapatite is beneficial for protein adsorption, preventing the activation of platelets [77, 78]. In addition, the number of platelets adhered on each surface was counted (Fig. 10c). Significantly fewer platelets were counted on the HA-patterned PLLA than on the pure PLLA ($p < 0.005$). This reduced adhesion on HA part than on the polymer part with the same surface area originated from the hemocompatibility of HA [50]. These results suggest that a vascular graft made of bioactive HA-patterned PLLA has a reduced possibility of occlusion or antithrombogenic potential and improved hemocompatibility [79-82].

2.4. Conclusions

A bioactive linear HA pattern was successfully fabricated and then transferred to a PLLA vascular graft using photolithography and solvent casting. The rough and porous surface of the HA pattern supported itself to be embedded tightly inside the polymer matrix, which resulted in better stability of the HA pattern on the PLLA surface than of the HA coating layer on the PLLA surface. Characteristic crystalline phases of HA were detected for the as-prepared HA pattern and HA pattern-transferred PLLA. Because of its intended application

as a vascular graft, the mechanical stability, *in vitro* endothelial cell behavior, and hemocompatibility of the HA-patterned sample were evaluated. Mechanical rolling-up, elongation, and *in vitro* circulation proved that the stability of the embedded HA pattern was superior to that of a simple HA coating layer on PLLA. Rapid endothelialization was observed on the HA-patterned PLLA in cell adhesion, migration, and proliferation tests. On the HA-patterned PLLA, the adhered endothelial cells were actively spread and elongated along the HA patterns, and the proliferation level was approximately twice as large as that for pure PLLA. Furthermore, the migration of endothelial cells was preferable on the HA-patterned PLLA. In addition, fewer adhered platelets were observed on the HA-patterned PLLA than on the pure PLLA. These findings suggest that HA-patterned PLLA can be utilized as a vascular graft.

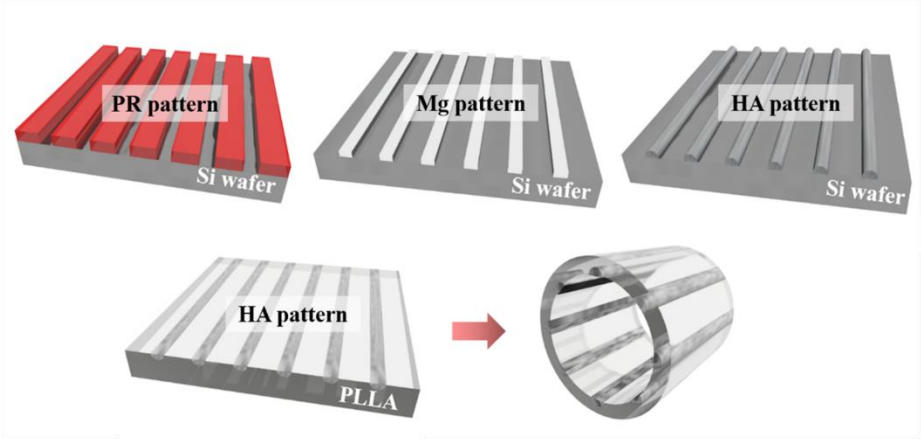

Figure 2.1. Schematic diagrams of HA patterning process by photolithography, pattern transferring process to PLLA film using solvent casting and the tubular shape of HA pattern transferred PLLA film.

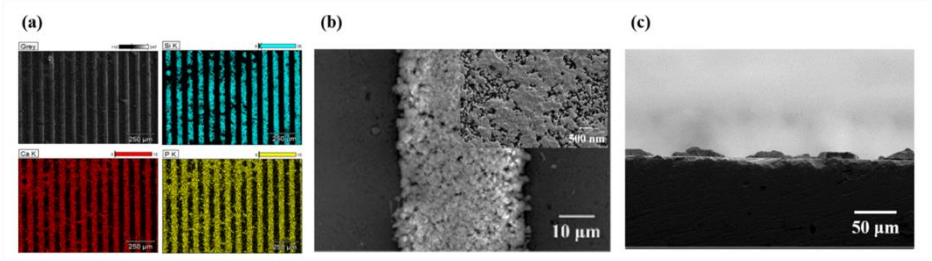

Figure 2.2. FE-SEM images of synthesized HA pattern on silicon wafer: A) FE-SEM and EDS mapping images of linear HA pattern on Si wafer, B) image of individual HA pattern and its highly magnified image, and C) cross-sectional image of HA pattern on the wafer. In the EDS mappings, cyan, red and yellow signals indicate Si, Ca and P, respectively.

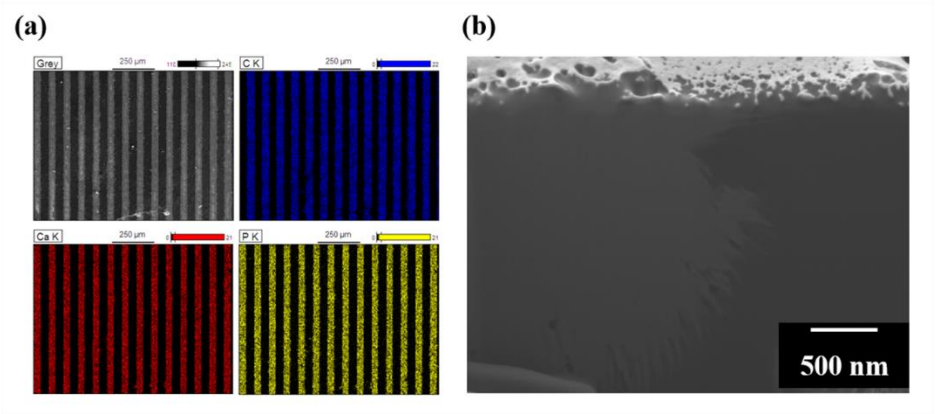

Figure 2.3. FE-SEM images of transferred HA pattern on PLLA matrix: A) low magnification FE-SEM and EDS images of HA patterned PLLA and B) cross-sectional image of HA pattern embedded inside PLLA matrix. In the EDS mappings, blue, red and yellow signals indicate C, Ca and P, respectively.

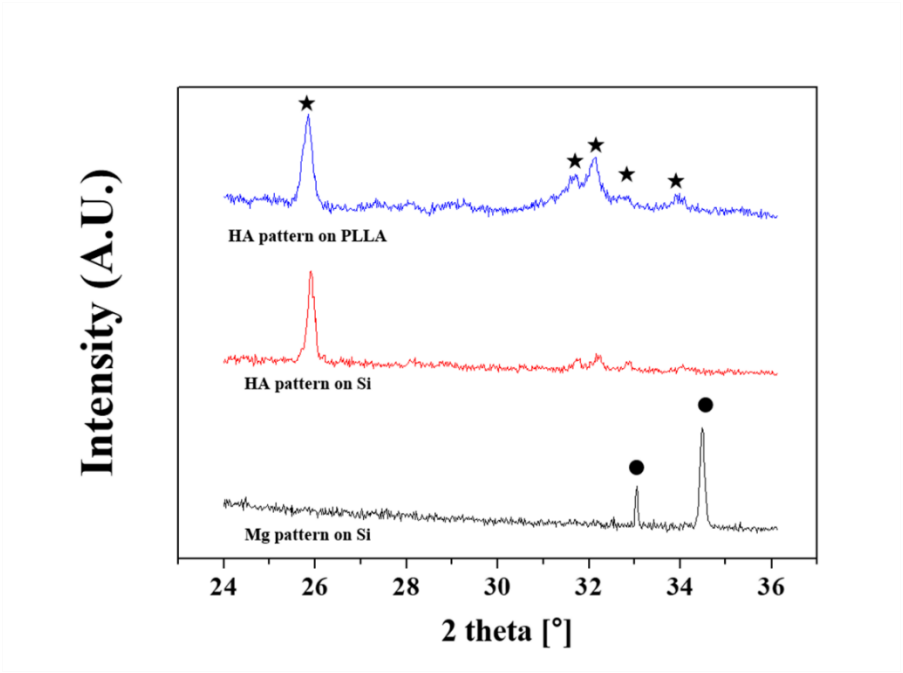

Figure 2.4. XRD patterns of Mg pattern on silicon wafer, HA pattern on silicon wafer, and HA- patterned PLLA (★:Hydroxyapatite ●:Magnesium).

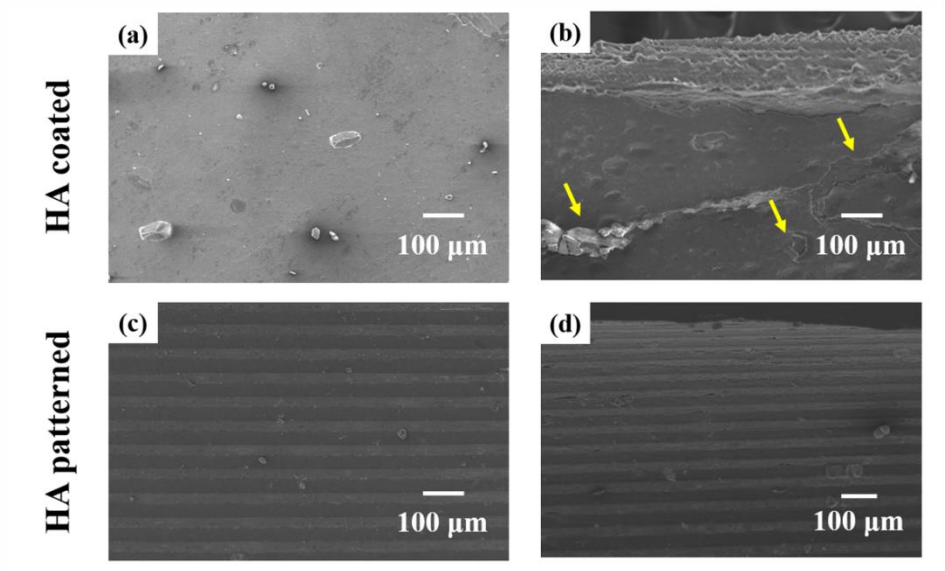

Figure 2.5. FE-SEM images of HA-coated and HA-patterned PLLA film before A), C) and after rolled up in tubular shape B, D).

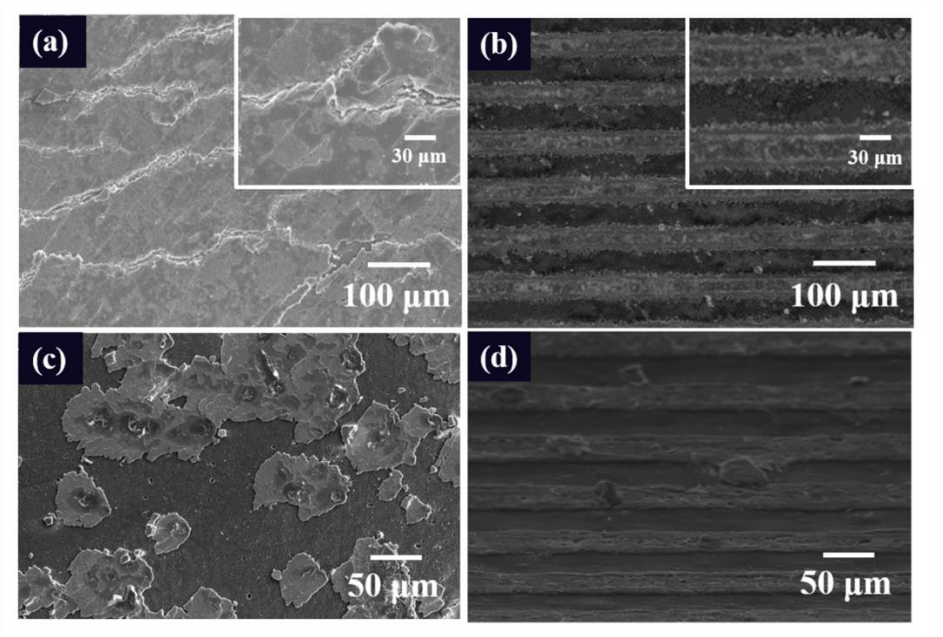

Figure 2.6. A) HA-coated and B) patterned PLLA after 5% elongation. Insets show high magnification images of each surface C) HA-coated and D) patterned PLLA after 4 weeks of *in vitro* circulation in DBPS medium.

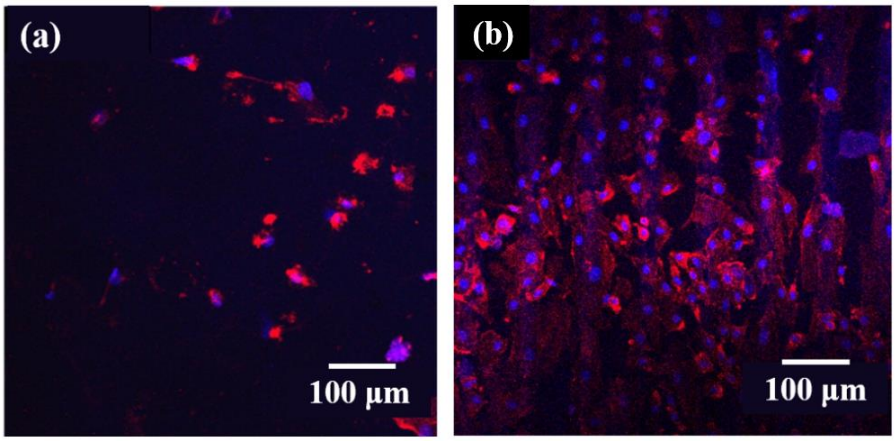

Figure 2.7. Representative CLSM images of HUVECs cultured on A) pure PLLA and B) HA-patterned PLLA after 24 hr.

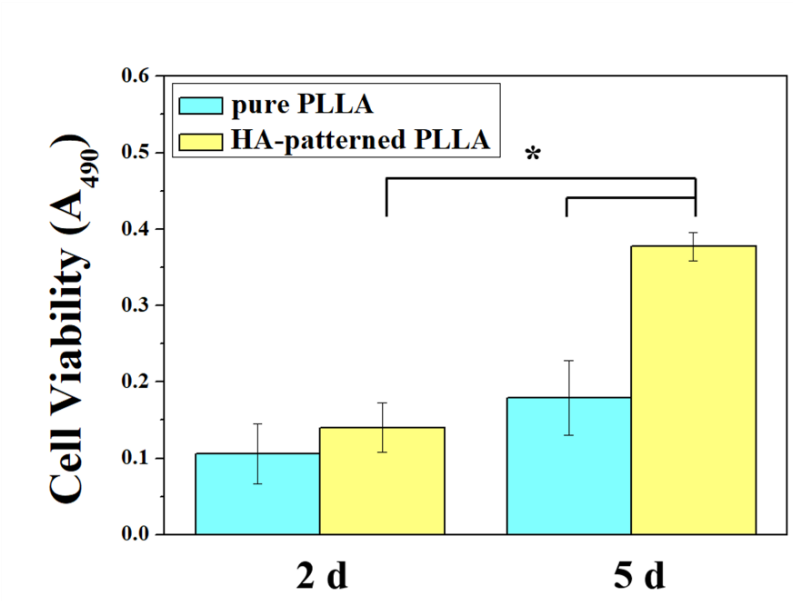

Figure 2.8. Levels of cell viability on pure and HA-patterned PLLA after 2 and 5 days (*$p < 0.05$).

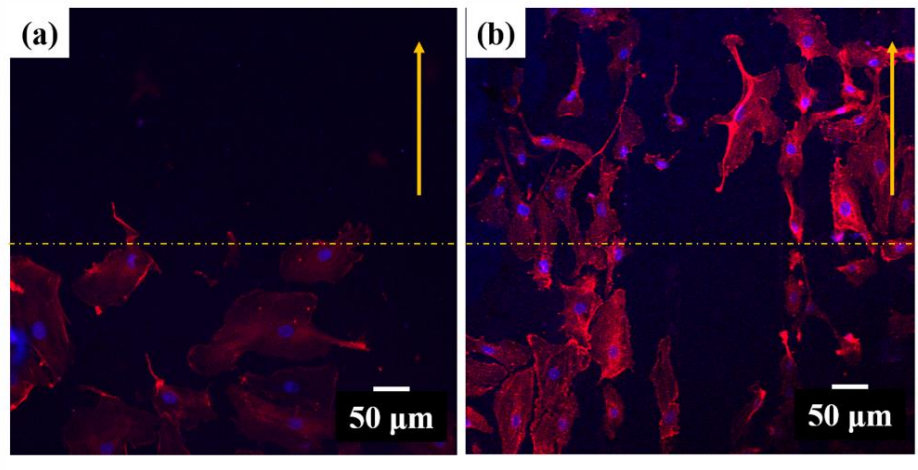

Figure 2.9. Representative CLSM images of HUVEC migration on A) pure and B) HA-patterned PLLA 24 hr after removing cell barrier (yellow arrow: migration direction, yellow dashed line: migration starting line).

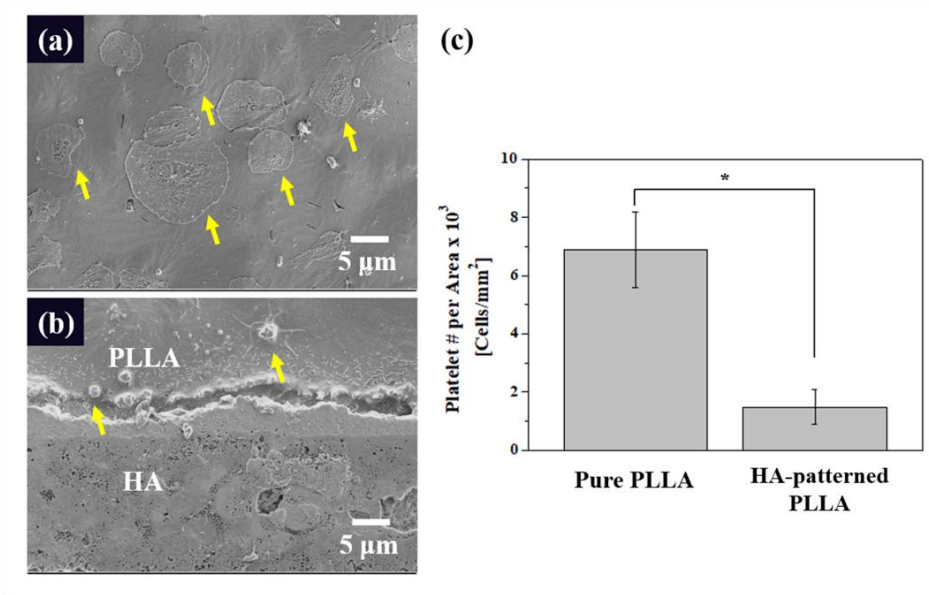

Figure 2.10. Representative FE-SEM images of platelets attached on A) pure and B) HA-patterned PLLA, and C) the number of platelets counted per area (yellow arrow: platelets, $*p < 0.05$).

Chapter 3.

High-dose drug loading system with HA pattern reservoir for guided bone regeneration

3.1. Introduction

GBR membranes are used as barriers to prevent soft tissue ingrowth in bone defects. Therefore, GBR membranes are crucial in periodontal therapy for guided tissue regeneration, which can effectively promote osseous regeneration [83-88].

Polymers are used for GBR membranes because of their flexibility and formability [89, 90]. Polymeric GBR membranes are divided into two main classes, degradable and non-degradable. e-PTFE is one of the most widely used non-degradable polymeric membranes. Despite its great mechanical properties, an e-PTFE GBR membrane requires a second surgery for removal. Furthermore, e-PTFE has poor biocompatibility, potentially leading to membrane exposure [88, 91]. Collagen, chitosan, and poly (lactic-co-glycolic acid) are degradable polymers that have good biocompatibility; however, their mechanical stiffness is not enough to maintain space for bone growth [92].

PLLA is also a biodegradable polymer and is one of the most widely studied in the biomedical field, especially GBR applications [93-97]. The mechanical stiffness of PLLA allows it to retain its original shape; moreover, its biocompatibility is better than that of other synthetic polymers. However, PLLA lacks osseoconductivity, limiting its application as a GBR membrane [98].

To improve osseoconductivity, different methods have been proposed to introduce osteoconductive HA into PLLA. A modified form of HA is found in bones; also, HA has great osseoconductivity, which is why it is widely found in GBR applications [83, 99, 100]. However, HA poorly binds to PLLA and is brittle, making it vulnerable to mechanical stimulus and fracture when it is coated on a PLLA surface. Therefore, in a previous work, we proposed a bio-ceramic pattern embedded in a polymer matrix to enhance the mechanical stability and improve the biocompatibility [101].

A simple method to further improve the biocompatibility of the polymeric materials is loading a growth factor into the matrix. Recombinant human bone morphogenetic protein-2 (rhBMP-2) is a promising growth factor for bone healing applications, including GBR membranes [90, 102-107]. Nevertheless, the hydrophobic PLLA surface is not adequate to couple with hydrophilic rhBMP-2, making it difficult to load the protein on the polymer without previous treatment. In contrast, HA has good affinity towards proteins and may therefore confer protein-loading ability in different matrices [28, 108, 109].

In this study, a HA pattern was embedded in a PLLA membrane and rhBMP-2 was loaded at the HA/PLLA interface, i.e., under the HA pattern (Fig.3.1). This is the first effort to modify the GBR membrane with embedding HA patterns for the structural stability. Meanwhile, no report has

been found on reporting embedded structure of micro patterns except some efforts introducing bioactive materials on the membrane surface. Hence, the high surface area of the hemispherical HA pattern can increase the rhBMP-2 loading amount. The HA layer was obtained by patterning magnesium via photolithography and converting it into HA by chemical treatment, then transferring it to PLLA by solvent casting. The morphology and stability of the pattern was characterized by FE-SEM and mechanical testing. The protein loading amount and the effect of rhBMP-2 were evaluated from green fluorescent protein (GFP) images and from the release profile of the growth factor. The influence of HA and rhBMP-2 on the biocompatibility of the PLLA membrane was investigated by the attachment, proliferation, and differentiation analysis of pre-osteoblasts. Additionally, in vivo testing based on a rabbit calvarial defect model allowed to assess the effect of HA and rhBMP-2 on the bone regeneration rate and maturity of bone tissue. Consequently, this study is suggesting the innovative method for drug delivery, promising for bone regeneration in GBR applications.

3.2. Experimental procedure

3.2.1. HA-patterned membrane fabrication

3.2.1.1. HA Patterning

A round HA pattern was fabricated using the same photolithography method with the first study. First, a 1.4-μm thick photoresist was spin-coated on the Si wafer. Then, a dot-shaped pattern (20-μm diameter) was introduced by exposing the photoresist layer to UV light through the precisely designed photomask. The UV-treated part was dissolved in a developer, and a round photoresist pattern with a diameter of 20 μm was generated. A 2-μm thick pure magnesium layer was then deposited on the patterned-photoresist layer using an electron-beam deposition. The Mg-deposited sample was then immersed into acetone to wash any remaining photoresist, leaving only the magnesium pattern on the Si wafer. This round Mg pattern was then converted into HA using an aqueous solution treatment, as previously described [54]. Briefly, the pattern was immersed in a 0.05 M Ca-EDTA/0.05 M KH_2PO_4 aqueous solution at 90 ℃ and pH 8.9 for 2 h. As magnesium reacts with water, hydroxyl ions were generated and combined with calcium and phosphate ions to yield HA.

3.2.1.2. Protein Loading

RhBMP-2 was selected as growth factor to demonstrate the potential of the HA-patterned membrane as a drug delivering GBR system. The lyophilized rhBMP-2 powder was dissolved in DPBS at a concentration of 10 μg/ml. To load the rhBMP-2, the Si wafer with the HA pattern was immersed

in the rhBMP-2 solution for 12 h at room temperature. Once the protein was absorbed on the surface, the sample was rinsed with DPBS three times and then dried.

3.2.1.3. HA Pattern Transfer

The rhBMP-2-loaded HA pattern was transferred to a polymer membrane by solvent casting. First, a 10 wt% PLLA/DCM solution was poured onto the patterned wafer. After evaporating the solvent, the PLLA membrane with the HA pattern was removed from the Si wafer surface (u/HAP). The membrane fabrication process is illustrated in Fig.3.1a.

Additionally, a pure PLLA membrane was fabricated by solvent casting (PLLA). A HA-patterned PLLA membrane without rhBMP-2 (HAP) was also prepared by solvent casting of PLLA on the HA-patterned Si wafer. A PLLA membrane with rhBMP-2 on top of the HA pattern (o/HAP) was fabricated by dipping the HAP sample into the rhBMP-2 solution (with the same concentration than for u/HAP). Each control group was used to verify the effect of the HA pattern, rhBMP-2, and drug loading site on the drug release behavior and cellular response (Fig.3.1b).

3.2.2. Surface characterization

The surface morphology and microstructure of the HA pattern and the pattern-transferred PLLA membrane were observed by FE-SEM.

3.2.3. Stability testing

The stability of the HA pattern on the PLLA membrane was investigated using two different mechanical stimuli, ultrasonication and tensile strain. A HA-patterned PLLA membrane (10 × 40 mm) was ultrasonicated in a bath type sonicator (WiseClean, Wisd, South Korea). Tensile strain (10%) was applied with a universal testing machine. After applying each mechanical stimulus, samples were examined by FE-SEM to observe any morphological changes on the surface.

3.2.4. Protein release behavior

To visualize the protein release behavior, GFP (produced using *E.coli*) was used instead of rhBMP-2. In addition, GFP was adsorbed onto the PLLA sample to confirm the effect of the HA pattern on the drug loading ability. The adsorbed GFP was then released in DPBS at 37 ℃ during 7 days. Remnant GFP on each sample was observed by CLSM.

The protein loading amount was quantified by obtaining the rhBMP-2 release profile from PLLA, o/HAP, and u/HAP. All samples were immersed

in DPBS at 37 ℃ and rhBMP-2 was released during 4 weeks to monitor the behavior. The absorbance of the released-rhBMP-2 solution was measured by UV spectroscopy (V-770, JASCO, USA) at 200 nm. The measured absorbance was quantified based on a calibration curve.

3.2.5. *In vitro* studies

The effects of the HA pattern and rhBMP-2 on the cellular behavior were monitored in terms of *in vitro* cell morphology, proliferation, and differentiation. The samples were cut into a square shape with a dimension of 10 × 10 mm for the cell adhesion and proliferation tests and 20 × 20 mm for the cell differentiation test. All specimens were sterilized by UV irradiation for 24 h prior to cell seeding. MC3T3-E1 was seeded onto each sample with a density of 2×10^4 cells/ml and cultured for 24 h. Afterwards, the cell-seeded samples were fixed in 4% paraformaldehyde for 10 min, rinsed three times with DPBS, and treated with 0.1% Triton X-100 for 5 min and 1% bovine serum albumin for 30 min. Then, the cells were stained with fluorescent Alexa Fluor 546 phalloidin for 20 min and 4′, 6-diamidino-2-phenylindole for 5 min. The cellular morphology was examined by CLSM.

The proliferation of the pre-osteoblasts was examined via the MTS assay. The amount of formazan, proportionate to the number of living cells,

was confirmed by measuring the absorbance at 490 nm with a micro-reader after three and five days of culturing (n = 4).

Finally, the osteoblastic differentiation was verified using an alkaline phosphatase (ALP) activity test. To induce the osteoblastic differentiation of pre-osteoblasts, 10 mM β-glycerophosphate and 50 μg/ml ascorbic acid were incorporated into the culture medium. After 14 days of culturing, the produced amount of p-nitrophenol was measured based on the absorbance at 405 nm on the micro-reader (n = 4).

3.2.6. *In vivo* animal experiments

The effects of HA pattern and rhBMP-2 on osseoconductivity were examined using a rabbit calvarial defect model. The in vivo experiments were performed according to the protocol approved by the Institutional Animal Care and Use Committee of Genoss (GEN-IACUC-1902-02). A total of specific-pathogen-free (SPF) grade New Zealand white male rabbits (12 weeks old, average weight of 3 kg) were obtained from a commercial supplier (KOSA Bion Inc., South Korea). All rabbits were weighed at the beginning and end of the experiment. They had a normal diet and were cared for under the same conditions.

Four types of membranes (PLLA, HAP, o/HAP, and u/HAP) were cut into 10 × 10 mm squares and sterilized under UV irradiation for 24 h prior to implantation. Surgical sites were shaved and treated with a surgical prep solution containing 10% povidone-iodine. The surgery was carried out under general anesthesia with 0.1 cc of 2% xylazine HCl, 0.2 cc of tiletamine HCl, and lidocaine. An incision of approximately 4 cm was created in the skin of the rabbit skull. An 8-mm diameter trephine bur was used to create defects on the calvaria. The membranes were then placed onto the defects and covered with the inner skin. Wounds were closed using surgical suture (n = 4).

After the operation, gentamicin (0.1 mg/kg) was injected every 24 h for three days. Animals were monitored daily for any adverse reaction. At six weeks following the implantation, animals were sacrificed by asphyxiation with carbon dioxide. The samples and surrounding tissues were harvested and fixed in 10% neutral buffered formalin.

3.2.7. Micro-CT analysis

The amount of regenerated bone in the calvarial defect was evaluated by micro computed tomography (micro-CT) analysis (Skyscan, 1173 micro-tomography System; Skyscan, Belgium) at a voltage of 100 kV and current of 80 μA. Scanned images were reconstructed using the manufacturer's software

(Brucker microCT, NRecon, Belgium). The volume of interest (VOI) was set in the calvarial defect region and the ratio of volume of regenerated bone to VOI was calculated with the CTAn software (Brucker microCT, Belgium).

3.2.8. Histological analysis

After decalcification in 4% ethylenediamine tetraacetic acid for 10 days, the extracted bones were washed, dehydrated with ethanol, and embedded in paraffin. The cross-sectional view of the bones in the fabricated paraffin blocks was exposed and cut into sections with 3-μm thickness (RM2235, Leica, Germany). Then, the sectioned specimens were stained using the Masson's trichrome method to clearly visualize newly formed bone. Microscopic images of the stained samples were acquired with a digital slide scanner (Panoramic 250 Flash III, 3DHISTECH Ltd., Hungary). The quantitative analysis of histological images was carried out using an image analyzing software (ImageJ, National Institute of Health, USA).

3.2.9. Statistical analysis

The statistical analysis was performed using IBM SPSS statistics 23 software (IBM, USA). Data are shown as the mean ± standard error deviation. Statistical analysis was performed using a one-way analysis of variance

(ANOVA), and p values less than 0.05 were considered statistically significant.

3.3. Results and discussion

3.3.1. Surface characterization

Fig.3.2 presents the SEM images of the as-fabricated HA pattern and HA-embedded PLLA. HA dots with a diameter of about 20 μm were successfully created on a Si wafer without any debris. The inset corresponds to an individual HA dot, showing its rough surface, which is due to the needle-like shape of HA crystals [110, 111]. In addition, there are micropores on its surface that would be adequate sites for drug loading. This rough morphology could also be beneficial for interlocking the HA dots and polymer matrix [112].

The HA pattern was then transferred to the PLLA matrix (HAP) as shown in Fig.3.2b. The HA dots were tightly embedded inside the polymer matrix with no gaps between the pattern and the matrix. Interestingly, each dot had a round dent on its center. This was attributed to the HA removal process. When peeling the HA pattern from the Si wafer, unreacted magnesium parts remained on the surface of the wafer. The remaining magnesium were imprinted on the center of transferred HA patterns as dents.

The amount of unreacted magnesium could be reduced by increasing the reaction time. However, full conversion of magnesium to HA results in a smooth HA dot surface, which would affect the drug loading. Therefore, 1 h was selected as the optimum reaction time to achieve a porous HA surface with sufficient HA conversion.

Additionally, Fig3.2c and 3.2d represent the morphology of drug loaded with HA patterns on PLLA membrane. Fig.3.2c stands for o/HAP, which is the sample with rhBMP-2 loaded on the transferred HA pattern and Fig.3.2d corresponds to u/HAP, which is the one with rhBMP-2 loaded under the HA pattern. In both images, no particular difference was notable compared with HAP (Fig.3.2b), meaning the loaded protein does not affect negatively on the transfer of HA patterns on the polymer matrix.

3.3.2. Mechanical stability

The SEM images in Fig.3.3a and 3.3b present the morphology of the HA-embedded PLLA membrane after sonication and tensile tests, respectively. The sonication test was performed at half the maximum power of an ultrasonic cleaner. The power was not quantified, but the conditions were harsher than normal physiological ones. Even after 30 min of sonication, most HA dots remained on their original positions (Fig.3.3a). Furthermore, a

tensile strain of 10% was applied to the HA-embedded PLLA to investigate its stability under mechanical deformation. The SEM image was obtained after the tensile load was removed (Fig.3.3b). HA dots remained on the PLLA matrix although an interfacial gap was generated in some of them. Under the harsh conditions of both experiments, HA dots remained firmly embedded inside the PLLA matrix. This demonstrates the mechanical stability of the HA pattern, which could positively contribute to cellular reaction and lead to successful bone regeneration.

3.3.3. Protein release behavior

The growth factor release behavior was both qualitatively and quantitatively examined (Fig.3.4). First, the GFP loaded on each sample (PLLA, o/HAP and u/HAP) was visualized by CLSM before and after seven days of releasing (Fig.3.4a). PLLA showed a weak fluorescent signal compared to the other samples. This low affinity towards the protein is explained by the lack of functional groups on the polymer surface [113]. The weakly bound proteins were rapidly released from the surface and no fluorescent signal was observed on day seven. Contrastingly, both HAP samples showed a strong fluorescent signal even on day zero. Moreover, GFP preferentially attached to the HA pattern rather than to the PLLA matrix,

proving the high affinity between HA and the protein. The high affinity can be explained by the electrostatic interactions between Ca^{2+} ions on HA and COO^- groups on proteins, and by hydrogen bonding between OH and PO_4^{3-} on HA and NH_2 residues of the protein [28, 109]. After seven days, the protein signal was still observed on u/HAP, whereas only a faint signal remained on o/HAP. This was attributed to the higher protein load amount on u/HAP compared to o/HAP.

Additionally, rhBMP-2 was loaded on the samples to quantitatively evaluate the protein release behavior for GBR application. The cumulative amounts of released rhBMP-2 were monitored for four weeks, as shown in Figure 4B. The total released amounts of rhBMP-2 from PLLA, o/HAP, and u/HAP were 1.48 ± 0.60, 2.75 ± 0.28, and 4.06 ± 0.59 μg, respectively. The amount of rhBMP-2 loading evidently increased with HA pattern, which confers increased protein affinity to PLLA. Comparing both HA patterned samples, the loading was higher on u/HAP. This can be attributed to the higher surface area of the hemispherical HA patterns compared to the flat HA patterns in o/HAP. The micro-rough and porous surface of HA was beneficial for protein adsorption (Fig.3.2a). Furthermore, even after four weeks, rhBMP-2 was still released from u/HAP at the highest amount, demonstrating the efficiency of the protein loading system. These results and those of the GFP release experiments indicate that the HA pattern on the PLLA matrix acted as

a drug carrying site for large loading. Thus, this drug delivery system, where proteins are under the HA pattern, can increase the protein loading efficiency and its persistence because of the structure and high protein affinity of the HA pattern [114].

3.3.4. *In vitro* biological properties

The biological properties were analyzed by three *in vitro* tests: attachment, proliferation, and differentiation of preosteoblasts (MC3T3-E1). The morphology of the attached cells for each sample was monitored by CLSM after 24 h of incubation (Fig.3.5). On the bare PLLA membrane, only a small number of preosteoblast cells with shrunk morphology appeared (Fig.3.5a). The shrunk structures indicate a lack of activation, which could lead to cell apoptosis [115]. Such poor cellular reaction on PLLA was mainly attributed to the low cell adhesion due to hydrophobicity and low protein adsorption of PLLA [113, 116].

The cells attached to HA-patterned samples showed actively spread shapes, regardless of the presence of rhBMP-2 (Fig.3.5b–d). In addition, the number of cells was much larger on HAP, o/HAP, and u/HAP compared with PLLA, but there was no difference between these three samples. The enhanced initial cell affinity of HA-patterned samples resulted from the

introduction of bioactive HA, which has high affinity towards cell-friendly proteins [108].

Osteoblastic proliferation and differentiation are depicted in Fig.3.6a and 3.6b, respectively. Three days of incubation were too short to demonstrate a significant difference in proliferation. Statistically significant differences were observed after five days. Consistent with the results of initial cell attachment, HA containing samples (HAP, o/HAP, and u/HAP) showed significantly higher proliferation than PLLA, regardless of the presence of rhBMP-2. It is interesting that neither initial attachment nor proliferation were affected by rhBMP-2. However, it is known that rhBMP-2 has a critical impact on osteoblastic differentiation but less or no impact on cell attachment or proliferation [117, 118].

After 14 days of culturing, the protein related to differentiation was indirectly measured using an ALP test kit. HAP and o/HAP demonstrated significantly higher differentiation compared to PLLA ($p<0.05$). HAP improved the differentiation when the HA pattern is on its surface. Although o/HAP samples were loaded with rhBMP-2, loosely bound rhBMP-2 was rapidly released from the HA surface, which explains the similar differentiation level compared to HAP. The differentiation was further enhanced in u/HAP samples compared with PLLA ($p < 0.005$), it was even higher than that of HAP and o/HAP ($p < 0.05$). Such enhancement can be

explained by a synergistic effect of the bioactive HA pattern and sustained release of rhBMP-2. During 14 days of culturing, the osteogenic culture medium was changed every three days, removing the released rhBMP-2. In summary, preosteoblast cells differentiation was larger on u/HAP that releases more rhBMP-2 than o/HAP.

3.3.5. *In vivo* animal experiments

Osseoconductivity of the GBR membrane was examined using a rabbit calvarial defect model. After six weeks of monitoring, the harvested tissues were visualized by micro-CT. According to the 3D reconstructed images, newly regenerated bones on the implantation sites partially covered the defects for all samples, Fig.3.7a. The amount of regenerated bone, however, was very small for the PLLA samples, only at the marginal area of the defect site. Compared with bare PLLA, the amount of regenerated bone was higher in HA-patterned membrane samples, covering a much larger area of the calvarial defect. This revealed that the HA pattern effectively improved the osseoconductivity of the PLLA membrane [119-121].

A quantitative analysis for bone regeneration was conducted with a CT analyzing program. The percentage of recovered bone for each group is presented in Fig.3.7b. As inferred from Fig.3.7a, the HA pattern samples

(HAP, o/HAP, and u/HAP) had a statistically higher percentage of regenerated bone ($p < 0.05$). However, no significant difference was noticed between HAP and o/HAP. This could be inferred from ALP expression (Fig.3.6b) because osteoblastic differentiation is closely linked to bone regeneration [122]. Less loading amount and fast release of rhBMP-2 on the o/HAP samples did not lead to further bone regeneration than the HAP group. However, bone regeneration on u/HAP was significantly higher than with any other samples ($p < 0.05$), as anticipated from the ALP activity results. During the six weeks of implantation, rhBMP-2 would be released from both o/HAP and u/HAP. However, as demonstrated in Fig.3.4, u/HAP displayed a sustained release and a higher loading amount compared with o/HAP group. The steady release of a larger amount of rhBMP-2 from u/HAP could thus result in the greater bone regeneration during the healing period.

Histological staining with the Masson's trichrome method was also carried out to visualize the maturation of regenerated bone on the defect sites (Fig.3.8). In the overall images (Fig.3.8a–d), the 8-mm-defect and recovered tissue are clearly represented. When using the bare PLLA membrane, only a little amount of bone was regenerated from the original defect location (Fig.3.8a and 3.8e). Soft connective tissue, stained in light blue, also filled the inside of the defect, instead of new bone. With HAP and o/HAP (Fig.3.8f and 3.8g), a light blue connective tissue layer also appeared inside the defect.

However, newly formed bone (deep cyan blue) embedded with numerous osteocytes was also observed in the middle of the defect. For the u/HAP membrane (Fig.3.8h), the portion of regenerated bone was much higher than that of soft tissue. Furthermore, the bone was stained with a deeper blue hue, indicating that new bone was more mature than in the other samples [114]. The amount of regenerated bone was quantified based on the histological images (Fig.3.9). Consistent with the micro-CT analysis, the percentage of recovered bone was the highest on u/HAP. However, the difference among the three samples (PLLA, HAP, and o/HAP) was not statistically significant.

The effects of HA pattern and rhBMP-2 on bone regeneration were consistent with the results of the *in vitro* cell tests. The presence of HA pattern affected the bone regeneration ability of the PLLA membrane. Moreover, the efficient delivery of rhBMP-2 further promoted the regeneration and maturation of new bone. The presence of osteoconductive HA along with the controlled release of rhBMP-2, synergistically enhanced bone regeneration.

3.4. Conclusions

In the second research, we developed a PLLA GBR membrane which was incorporated with dot-shaped HA patterns and rhBMP-2 under the

pattern for improved osseoconductivity. The HA dots, obtained from Mg, had a rough surface that are anticipated to allow for strong interlocking with the PLLA matrix. Ultra-sonication and tensile testing verified that the transferred HA pattern was mechanically stable in harsh conditions. Protein loading ability tests using GFP and rhBMP-2 clearly revealed that the protein was effectively loaded on the PLLA membrane with HA pattern, unlike bare PLLA in which loading was not observed. Furthermore, a larger amount of protein could be loaded under the HA pattern (u/HAP) compared to on top of the HA pattern (o/HAP). Also, u/HAP showed a more controlled protein release profile than bare PLLA and o/HAP. The HA pattern and controlled release of rhBMP-2 synergistically affected the osteogenic properties of the PLLA membrane.

In vitro cellular tests using preosteoblasts showed that u/HAP had an enhanced ALP activity compared to PLLA, HAP (HA pattern without rhBMP-2) and o/HAP groups. *In vivo* testings with a rabbit calvarial model also revealed that u/HAP had significantly improved bone regenerating abilities. Both micro-CT and histological analysis indicate the amount of new bone was significantly larger when applying u/HAP compared to the other membranes. Moreover, the new bone was more mature in the u/HAP, demonstrated by the staining color in the histological images. These results

suggest that the HA pattern with rhBMP-2 under it would improve the potential of polymer membranes for GBR applications.

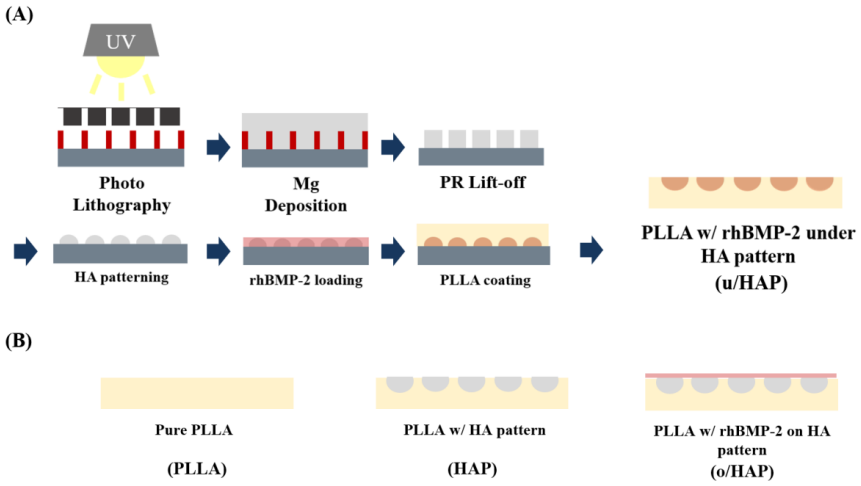

Figure 3.1. Scheme of A) HA and drug patterning on the PLLA film by photolithography and B) control groups.

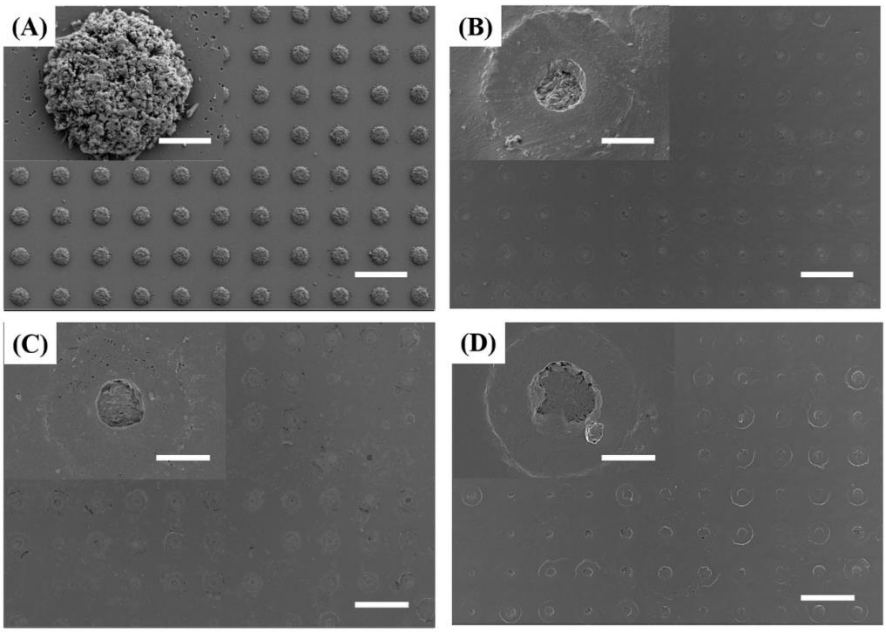

Figure 3.2. FE-SEM images of A) synthesized HA pattern on silicon wafer and B) transferred HA pattern on PLLA matrix (HAP), C) rhBMP-2 loaded on the transferred HA pattern(o/HAP), and D) rhBMP-2 loaded under the transferred HA pattern(u/HAP) (scale: 50 μm, inset scale: 10 μm).

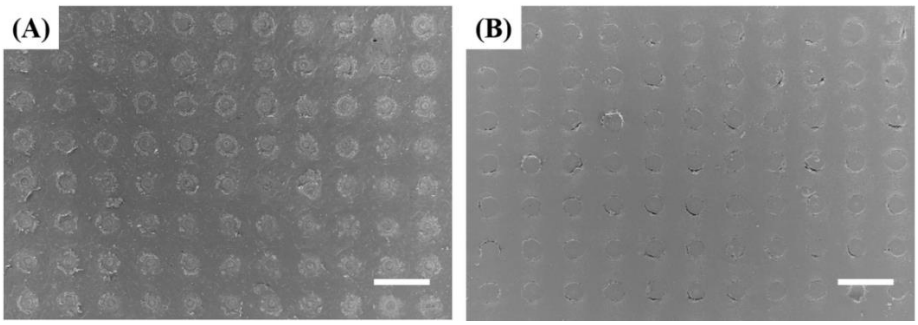

Figure 3.3. FE-SEM images of HA-embedded PLLA film after A) sonication and B) 10% strain tensile tests (scale bar: 50 μm).

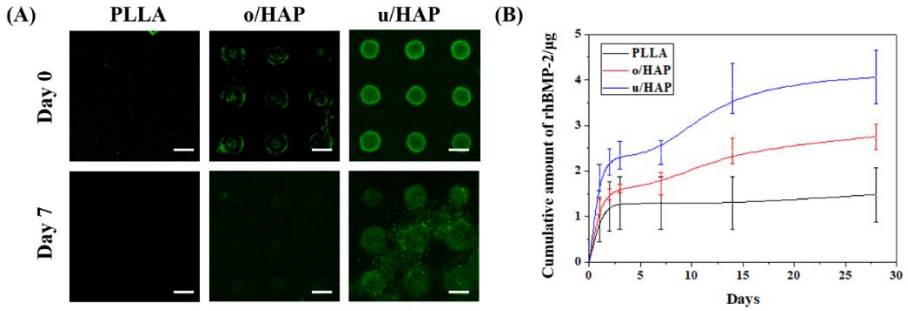

Figure 3.4. A) CLSM images of GFP-loaded on PLLA, o/HAP, and u/HAP before and after 7 days of release in DPBS (scale bar: 30 μm). B) rhBMP-2 release profile of rhBMP-2 loaded on PLLA, o/HAP, and u/HAP (n = 5).

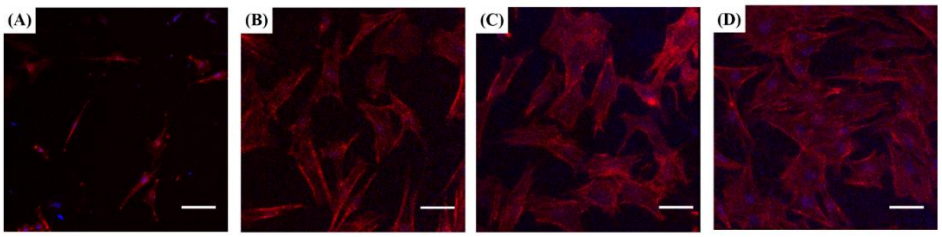

Figure 3.5. CLSM images of MC3T3-E1 on A) PLLA, B) HAP, C) o/HAP, and D) u/HAP samples after culturing for 24 h (scale bar: 50 μm).

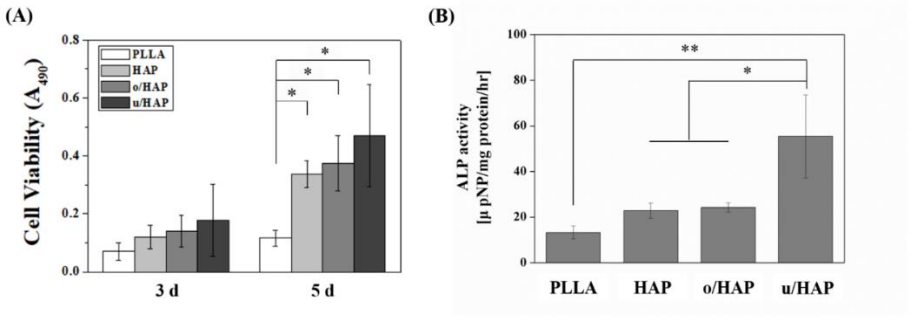

Figure 3.6. Representative A) levels of cell viability and B) ALP activity on PLLA, HAP, o/HAP, and u/HAP (n=4, *$p < 0.05$, **$p < 0.005$).

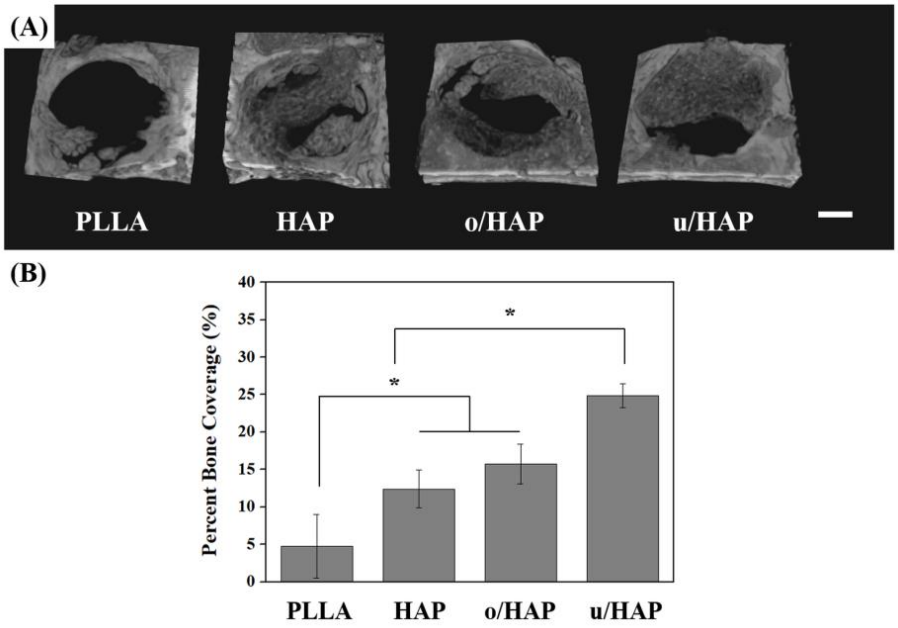

Figure 3.7. A) Representative micro-CT images of harvested rabbit calvaria with PLLA, HAP, o/HAP, and u/HAP after six weeks (scale bar: 2 mm). B) Percentage of bone coverage on each defect ($n = 3$, $*p < 0.05$).

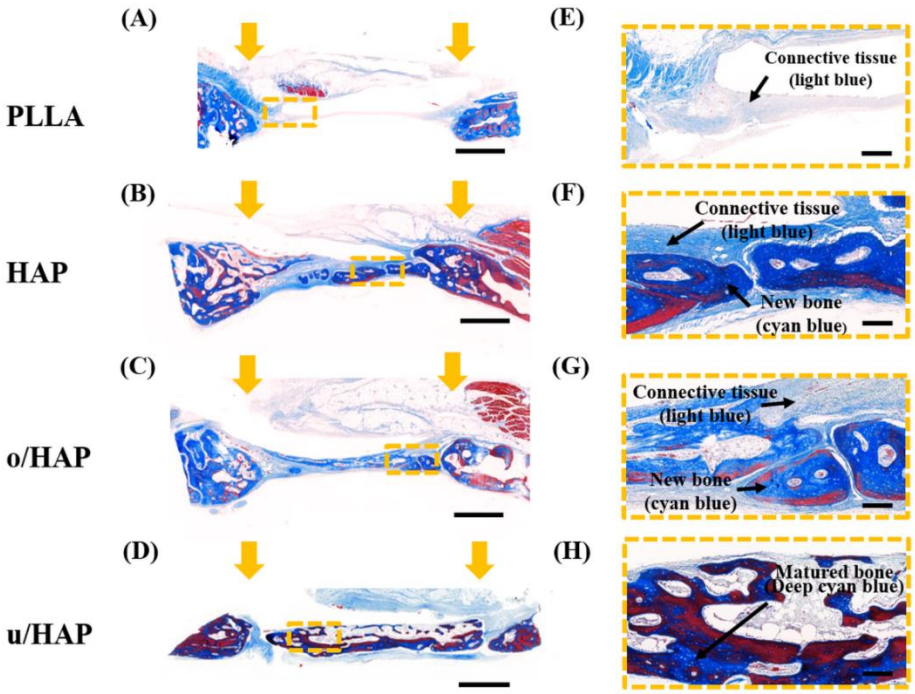

Figure 3.8. Histological images stained with Masson's trichrome. (A–D) Overall view of regenerated calvarial tissue six weeks after implantation (scale bar: 2 mm). (E–H) Highly magnified images of regenerated tissue portions highlighted in orange in (A–D) (scale bar: 200 μm).

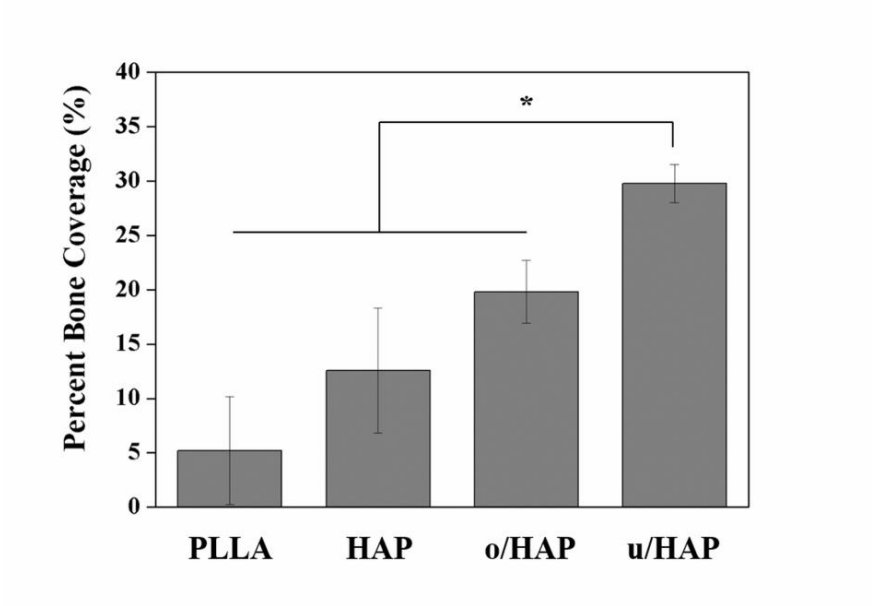

Figure 3.9. Percentage of bone coverage on each sample six weeks after implantation based on the histological images (stained with Masson's Trichrome, n = 3, *p < 0.05).

Chapter 4.

Conclusions

4.1. Conclusions

This thesis is targeting on improving biological properties of polymer-based scaffold for further applications via bioactive HA micro-patterning and transferring in various tissue engineering applications. As different requirements emerge depending on the various implantation sites, different biological functions are necessary.

In chapter 2, PLLA vascular graft with linear HA micro-pattern was fabricated. The micro-patterns were successfully fabricated and transferred on the PLLA membrane with embedded structure. The crystalline phase of HA was revealed after HA conversion process and not affected during the transfer. The patterned shape was not demolished or deformed during various stability testing. Furthermore, the series of *in vitro* cell and platelet tests demonstrated that this system was promising substitute for the existing vascular graft.

Chapter 3 focused on drug loading on the round HA pattern for the application of GBR membrane. Employing the distinctive structure of patterning and transferring system, rhBMP-2, inducing bone formation was incorporated under the HA pattern. The successful HA transferring was confirmed with or without rhBMP-2 loading. Mechanical stability of HA-patterned membrane was identified via stability testing. The remarkable protein loading amount on the experimental group was illustrated by the series of

protein loading and releasing tests. *In vitro* biocompatibility and osteoblastic differentiation tests were performed to evaluate the effect of HA and loaded rhBMP-2. In terms of bone regeneration, *in vivo* tests were decisive to estimate the amount of newly formed bone.

In conclusion, this study suggested diverse strategies including bioactive material patterning, cell guiding effect, and drug delivery that offers great potential for biomedical applications. Based on these researches, various properties could be obtained that is appropriate for specific implantation sites. And further researches could be performed regarding micro-patterning of different kinds of material in various medical applications.

References

[1] X. Liu, P.X. Ma, Polymeric Scaffolds for Bone Tissue Engineering, Ann Biomed Eng, 32 (2004) 477-486.

[2] K.Y. Lee, D.J. Mooney, Hydrogels for Tissue Engineering, Chemical Reviews, 101 (2001) 1869-1880.

[3] J. Rouwkema, N.C. Rivron, C.A. van Blitterswijk, Vascularization in tissue engineering, Trends in Biotechnology, 26 (2008) 434-441.

[4] E.S. Place, N.D. Evans, M.M. Stevens, Complexity in biomaterials for tissue engineering, Nature Materials, 8 (2009) 457-470.

[5] P.X. Ma, Biomimetic materials for tissue engineering, Adv Drug Deliver Rev, 60 (2008) 184-198.

[6] F.J. O'Brien, Biomaterials & scaffolds for tissue engineering, Materials Today, 14 (2011) 88-95.

[7] S. Naahidi, M. Jafari, M. Logan, Y. Wang, Y. Yuan, H. Bae, B. Dixon, P. Chen, Biocompatibility of hydrogel-based scaffolds for tissue engineering applications, Biotechnology Advances, 35 (2017) 530-544.

[8] Y. Pang, A. Qin, X. Lin, L. Yang, Q. Wang, Z. Wang, Z. Shan, S. Li, J. Wang, S. Fan, Q. Hu, Biodegradable and biocompatible high elastic chitosan scaffold is cell-friendly both in vitro and in vivo, Oncotarget, 8

(2017) 35583-35591.

[9] G.-Z. Jin, T.-H. Kim, J.-H. Kim, J.-E. Won, S.-Y. Yoo, S.-J. Choi, J.K. Hyun, H.-W. Kim, Bone tissue engineering of induced pluripotent stem cells cultured with macrochanneled polymer scaffold, J Biomed Mater Res A, 101A (2013) 1283-1291.

[10] K. Rezwan, Q.Z. Chen, J.J. Blaker, A.R. Boccaccini, Biodegradable and bioactive porous polymer/inorganic composite scaffolds for bone tissue engineering, Biomaterials, 27 (2006) 3413-3431.

[11] J. Guan, K.L. Fujimoto, M.S. Sacks, W.R. Wagner, Preparation and characterization of highly porous, biodegradable polyurethane scaffolds for soft tissue applications, Biomaterials, 26 (2005) 3961-3971.

[12] C. Xu, F. Yang, S. Wang, S. Ramakrishna, In vitro study of human vascular endothelial cell function on materials with various surface roughness, J Biomed Mater Res A, 71A (2004) 154-161.

[13] S. Sarkar, K.M. Sales, G. Hamilton, A.M. Seifalian, Addressing thrombogenicity in vascular graft construction, Journal of Biomedical Materials Research Part B: Applied Biomaterials, 82B (2007) 100-108.

[14] G. Wei, P.X. Ma, Structure and properties of nano-hydroxyapatite/polymer composite scaffolds for bone tissue engineering,

Biomaterials, 25 (2004) 4749-4757.

[15] D.-Y. Ji, T.-F. Kuo, H.-D. Wu, J.-C. Yang, S.-Y. Lee, A novel injectable chitosan/polyglutamate polyelectrolyte complex hydrogel with hydroxyapatite for soft-tissue augmentation, Carbohydrate Polymers, 89 (2012) 1123-1130.

[16] C.J. Au - Wilcock, P. Au - Gentile, P.V. Au - Hatton, C.A. Au - Miller, Rapid Mix Preparation of Bioinspired Nanoscale Hydroxyapatite for Biomedical Applications, JoVE, DOI doi:10.3791/55343(2017) e55343.

[17] D. Bellucci, A. Sola, A. Anesi, R. Salvatori, L. Chiarini, V. Cannillo, Bioactive glass/hydroxyapatite composites: Mechanical properties and biological evaluation, Materials Science and Engineering: C, 51 (2015) 196-205.

[18] M. Ogiso, Y. Yamashita, T. Matsumoto, The Process of Physical Weakening and Dissolution of the HA-coated Implant in Bone and Soft Tissue, J Dent Res, 77 (1998) 1426-1434.

[19] I. Vasiev, A.I.M. Greer, A.Z. Khokhar, J. Stormonth-Darling, K.E. Tanner, N. Gadegaard, Self-folding nano- and micropatterned hydrogel tissue engineering scaffolds by single step photolithographic process, Microelectronic Engineering, 108 (2013) 76-81.

[20] C. Hallgren, H. Reimers, J. Gold, A. Wennerberg, The importance of surface texture for bone integration of screw shaped implants: An in vivo study of implants patterned by photolithography, J Biomed Mater Res, 57 (2001) 485-496.

[21] T. Limongi, R. Schipani, A. Di Vito, A. Giugni, M. Francardi, B. Torre, M. Allione, E. Miele, N. Malara, S. Alrasheed, R. Raimondo, P. Candeloro, V. Mollace, E. Di Fabrizio, Photolithography and micromolding techniques for the realization of 3D polycaprolactone scaffolds for tissue engineering applications, Microelectronic Engineering, 141 (2015) 135-139.

[22] G. De Visscher, L. Mesure, B. Meuris, A. Ivanova, W. Flameng, Improved endothelialization and reduced thrombosis by coating a synthetic vascular graft with fibronectin and stem cell homing factor SDF-1α, Acta Biomater, 8 (2012) 1330-1338.

[23] V. Janakiraman, B.L. Kienitz, H. Baskaran, Lithography Technique for Topographical Micropatterning of Collagen-Glycosaminoglycan Membranes for Tissue Engineering Applications, Journal of Medical Devices, 1 (2007) 233-237.

[24] Y. Li, G. Huang, X. Zhang, L. Wang, Y. Du, T.J. Lu, F. Xu,

Engineering cell alignment in vitro, Biotechnology Advances, 32 (2014) 347-365.

[25] Y. Lu, S.C. Chen, Micro and nano-fabrication of biodegradable polymers for drug delivery, Adv Drug Deliver Rev, 56 (2004) 1621-1633.

[26] T.J. Sill, H.A. von Recum, Electrospinning: Applications in drug delivery and tissue engineering, Biomaterials, 29 (2008) 1989-2006.

[27] X. Hu, S. Liu, G. Zhou, Y. Huang, Z. Xie, X. Jing, Electrospinning of polymeric nanofibers for drug delivery applications, J Control Release, 185 (2014) 12-21.

[28] X. Dong, Q. Wang, T. Wu, H. Pan, Understanding Adsorption-Desorption Dynamics of BMP-2 on Hydroxyapatite (001) Surface, Biophysical Journal, 93 (2007) 750-759.

[29] R.M. Nerem, D. Seliktar, Vascular Tissue Engineering, Annual Review of Biomedical Engineering, 3 (2001) 225-243.

[30] N.F. Huang, S. Li, Mesenchymal stem cells for vascular regeneration, Regen Med, 3 (2008) 877-892.

[31] T. Gong, K. Zhao, X. Liu, L. Lu, D. Liu, S. Zhou, A Dynamically Tunable, Bioinspired Micropatterned Surface Regulates Vascular Endothelial and Smooth Muscle Cells Growth at Vascularization, Small,

12 (2016) 5769-5778.

[32] R.E. Gerszten, T.J. Wang, The search for new cardiovascular biomarkers, Nature, 451 (2008) 949.

[33] S.L. Mitchell, L.E. Niklason, Requirements for growing tissue-engineered vascular grafts, Cardiovascular Pathology, 12 (2003) 59-64.

[34] B. Jiang, R. Suen, J.-J. Wang, Z.J. Zhang, J.A. Wertheim, G.A. Ameer, Vascular scaffolds with enhanced antioxidant activity inhibit graft calcification, Biomaterials, 144 (2017) 166-175.

[35] G.W. Bos, A.A. Poot, T. Beugeling, W.G. van Aken, J. Feijen, Small-Diameter Vascular Graft Prostheses: Current Status, Archives of Physiology and Biochemistry, 106 (1998) 100-115.

[36] L. Xue, H.P. Greisler, Biomaterials in the development and future of vascular grafts, J Vasc Surg, 37 (2003) 472-480.

[37] M. Chaouat, C. Le Visage, W.E. Baille, B. Escoubet, F. Chaubet, M.A. Mateescu, D. Letourneur, A Novel Cross-linked Poly(vinyl alcohol) (PVA) for Vascular Grafts, Advanced Functional Materials, 18 (2008) 2855-2861.

[38] D.C. Miller, A. Thapa, K.M. Haberstroh, T.J. Webster, Endothelial and vascular smooth muscle cell function on poly(lactic-co-glycolic acid)

with nano-structured surface features, Biomaterials, 25 (2004) 53-61.

[39] M.C. Serrano, M.T. Portolés, M. Vallet-Regí, I. Izquierdo, L. Galletti, J.V. Comas, R. Pagani, Vascular Endothelial and Smooth Muscle Cell Culture on NaOH-Treated Poly(ε-caprolactone) Films: A Preliminary Study for Vascular Graft Development, Macromolecular Bioscience, 5 (2005) 415-423.

[40] C.P. Barnes, S.A. Sell, E.D. Boland, D.G. Simpson, G.L. Bowlin, Nanofiber technology: Designing the next generation of tissue engineering scaffolds, Adv Drug Deliver Rev, 59 (2007) 1413-1433.

[41] T. Sugiura, S. Tara, H. Nakayama, T. Yi, Y.-U. Lee, T. Shoji, C.K. Breuer, T. Shinoka, Fast-degrading bioresorbable arterial vascular graft with high cellular infiltration inhibits calcification of the graft, J Vasc Surg, 66 (2017) 243-250.

[42] S. de Valence, J.-C. Tille, D. Mugnai, W. Mrowczynski, R. Gurny, M. Möller, B.H. Walpoth, Long term performance of polycaprolactone vascular grafts in a rat abdominal aorta replacement model, Biomaterials, 33 (2012) 38-47.

[43] W. He, T. Yong, W.E. Teo, Z. Ma, S. Ramakrishna, Fabrication and Endothelialization of Collagen-Blended Biodegradable Polymer

Nanofibers: Potential Vascular Graft for Blood Vessel Tissue Engineering, Tissue Eng, 11 (2005) 1574-1588.

[44] H.-C. Wu, T.-W. Wang, P.-L. Kang, Y.-H. Tsuang, J.-S. Sun, F.-H. Lin, Coculture of endothelial and smooth muscle cells on a collagen membrane in the development of a small-diameter vascular graft, Biomaterials, 28 (2007) 1385-1392.

[45] J.H. Lee, Y. Lee Keun, K. Gupta Manoj, Y. Kim Tae, D.Y. Lee, J. Oh, C. Ryu, J. Yoo Won, C.Y. Kang, S.J. Yoon, J.B. Yoo, S.W. Kim, Highly Stretchable Piezoelectric-Pyroelectric Hybrid Nanogenerator, Advanced Materials, 26 (2013) 765-769.

[46] Q.F. Tu, Y.C. Zhao, X.Q. Xue, J. Wang, N. Huang, Improved Endothelialization of Titanium Vascular Implants by Extracellular Matrix Secreted from Endothelial Cells, Tissue Engineering Part A, 16 (2010) 3635-3645.

[47] K. Liu, N. Wang, W. Wang, L. Shi, H. Li, F. Guo, L. Zhang, L. Kong, S. Wang, Y. Zhao, A bio-inspired high strength three-layer nanofiber vascular graft with structure guided cell growth, J Mater Chem B, 5 (2017) 3758-3764.

[48] Z. Tan, X. Gao, T. Liu, Y. Yang, J. Zhong, C. Tong, Y. Tan,

Electrospun vein grafts with high cell infiltration for vascular tissue engineering, Materials Science and Engineering: C, 81 (2017) 407-415.

[49] H. Kadono, T. Furuzono, M. Masuda, M. Okada, M. Ueki, K. Takamizawa, R. Tanaka, K. Miyatake, Y. Koyama, K. Takakuda, In Vivo Evaluation of Hydroxyapatite Nanocoating on Polyester Artificial Vascular Grafts and Possibility as Soft-Tissue Compatible Material, Asaio J, 56 (2010) 61-66.

[50] T. Furuzono, M. Masuda, M. Okada, S. Yasuda, H. Kadono, R. Tanaka, K. Miyatake, Increase in Cell Adhesiveness on a Poly(ethylene terephthalate) Fabric by Sintered Hydroxyapatite Nanocrystal Coating in the Development of an Artificial Blood Vessel, Asaio J, 52 (2006) 315-320.

[51] A. Korematsu, T. Furuzono, S. Yasuda, J. Tanaka, A. Kishida, Nano-scaled hydroxyapatite/polymer composite III. Coating of sintered hydroxyapatite particles on poly(4-methacryloyloxyethyl trimellitate anhydride)-grafted silk fibroin fibers, Journal of Materials Science: Materials in Medicine, 16 (2005) 67-71.

[52] K. Wang, M. Wang, Q. Wang, X. Lu, X. Zhang, Computer simulation of proteins adsorption on hydroxyapatite surfaces with

calcium phosphate ions, Journal of the European Ceramic Society, 37 (2017) 2509-2520.

[53] K. Iijima, A. Iizuka, R. Suzuki, H. Ueno-Yokohata, N. Kiyokawa, M. Hashizume, Effect of protein adsorption layers and solution treatments on hydroxyapatite deposition on polystyrene plate surfaces in simulated body fluids, Journal of Materials Science: Materials in Medicine, 28 (2017) 193.

[54] S.-M. Kim, M.-H. Kang, H.-E. Kim, H.-K. Lim, S.-H. Byun, J.-H. Lee, S.-M. Lee, Innovative micro-textured hydroxyapatite and poly(l-lactic)-acid polymer composite film as a flexible, corrosion resistant, biocompatible, and bioactive coating for Mg implants, Materials Science and Engineering: C, 81 (2017) 97-103.

[55] J. Wang, L. Liu, Y. Wu, M.F. Maitz, Z. Wang, Y. Koo, A. Zhao, J. Sankar, D. Kong, N. Huang, Y. Yun, Ex vivo blood vessel bioreactor for analysis of the biodegradation of magnesium stent models with and without vessel wall integration, Acta Biomater, 50 (2017) 546-555.

[56] S.M. Kim, J.H. Jo, S.M. Lee, M.H. Kang, H.E. Kim, Y. Estrin, J.H. Lee, J.W. Lee, Y.H. Koh, Hydroxyapatite-coated magnesium implants with improved in vitro and in vivo biocorrosion, biocompatibility, and

bone response, J Biomed Mater Res A, 102 (2014) 429-441.

[57] M.J. Dalby, L. Di Silvio, E.J. Harper, W. Bonfield, Increasing hydroxyapatite incorporation into poly(methylmethacrylate) cement increases osteoblast adhesion and response, Biomaterials, 23 (2002) 569-576.

[58] J.R. Woodard, A.J. Hilldore, S.K. Lan, C.J. Park, A.W. Morgan, J.A.C. Eurell, S.G. Clark, M.B. Wheeler, R.D. Jamison, A.J. Wagoner Johnson, The mechanical properties and osteoconductivity of hydroxyapatite bone scaffolds with multi-scale porosity, Biomaterials, 28 (2007) 45-54.

[59] L.J. Cheng, F. Ye, R.N. Yang, X.F. Lu, Y.J. Shi, L. Li, H.S. Fan, H. Bu, Osteoinduction of hydroxyapatite/beta-tricalcium phosphate bioceramics in mice with a fractured fibula, Acta Biomater, 6 (2010) 1569-1574.

[60] J. Huang, J. Xiong, J. Liu, W. Zhu, D. Wang, Investigation of the In Vitro Degradation of a Novel Polylactide/Nanohydroxyapatite Composite for Artificial Bone, 2013.

[61] H.C. Urschel, Jr., M.A. Razzuk, M. Gardner, Coronary Artery Bypass Occlusion Secondary to Postcardiotomy Syndrome, The Annals

of Thoracic Surgery, 22 (1976) 528-531.

[62] M. Wei, A.J. Ruys, B.K. Milthorpe, C.C. Sorrell, Solution ripening of hydroxyapatite nanoparticles: Effects on electrophoretic deposition, J Biomed Mater Res, 45 (1999) 11-19.

[63] M.F. Zambaux, F. Bonneaux, R. Gref, E. Dellacherie, C. Vigneron, Preparation and characterization of protein C-loaded PLA nanoparticles, J Control Release, 60 (1999) 179-188.

[64] M.J.B. Wissink, R. Beernink, A.A. Poot, G.H.M. Engbers, T. Beugeling, W.G. van Aken, J. Feijen, Improved endothelialization of vascular grafts by local release of growth factor from heparinized collagen matrices, J Control Release, 64 (2000) 103-114.

[65] I. Adipurnama, M.C. Yang, T. Ciach, B. Butruk-Raszeja, Surface modification and endothelialization of polyurethane for vascular tissue engineering applications: a review, Biomater Sci-Uk, 5 (2017) 22-37.

[66] H.-F. Guo, W.-W. Dai, D.-H. Qian, Z.-X. Qin, Y. Lei, X.-Y. Hou, C. Wen, A simply prepared small-diameter artificial blood vessel that promotes in situ endothelialization, Acta Biomater, 54 (2017) 107-116.

[67] X. Ma, Y. Liu, X.M. Wu, C. Wang, Q. Li, T. Fu, Synthesis of europium-doped nanohydroxyapatite and its cytocompatibility with

endothelial cells in vitro, Materials Technology, 31 (2016) 23-27.

[68] S. Pezzatini, R. Solito, L. Morbidelli, S. Lamponi, E. Boanini, A. Bigi, M. Ziche, The effect of hydroxyapatite nanocrystals on microvascular endothelial cell viability and functions, J Biomed Mater Res A, 76A (2006) 656-663.

[69] S.V. Pislaru, A. Harbuzariu, G. Agarwal, T. Witt Aas Cvt Latg, R. Gulati, N.P. Sandhu, C. Mueske Aa, M. Kalra, R.D. Simari, G.S. Sandhu, Magnetic Forces Enable Rapid Endothelialization of Synthetic Vascular Grafts, Circulation, 114 (2006) I-314.

[70] K.M. Sedlarik, P.B. van Wachem, H. Bartels, J.M. Schakenraad, Rapid endothelialization of mieroporous vascular prostheses covered with meshed vascular tissue: a preliminary report, Biomaterials, 11 (1990) 4-8.

[71] J.L. Chen, Q.L. Li, J.G. Xu, L. Zhang, M.F. Maitz, J. Li, Thromboresistant and rapid-endothelialization effects of dopamine and staphylococcal protein A mediated anti-CD34 coating on 316L stainless steel for cardiovascular devices, J Mater Chem B, 3 (2015) 2615-2623.

[72] Y. Yao, J. Wang, Y. Cui, R. Xu, Z. Wang, J. Zhang, K. Wang, Y. Li, Q. Zhao, D. Kong, Effect of sustained heparin release from PCL/chitosan

hybrid small-diameter vascular grafts on anti-thrombogenic property and endothelialization, Acta Biomater, 10 (2014) 2739-2749.

[73] J. Shi, S. Chen, L. Wang, X. Zhang, J. Gao, L. Jiang, D. Tang, L. Zhang, A. Midgley, D. Kong, S. Wang, Rapid endothelialization and controlled smooth muscle regeneration by electrospun heparin-loaded polycaprolactone/gelatin hybrid vascular grafts, Journal of Biomedical Materials Research Part B: Applied Biomaterials, 0 (2018).

[74] T. Wu, J. Zhang, Y. Wang, B. Sun, M. Yin, G.L. Bowlin, X. Mo, Design and Fabrication of a Biomimetic Vascular Scaffold Promoting in Situ Endothelialization and Tunica Media Regeneration, ACS Applied Bio Materials, 1 (2018) 833-844.

[75] C.K. Hashi, Y. Zhu, G.-Y. Yang, W.L. Young, B.S. Hsiao, K. Wang, B. Chu, S. Li, Antithrombogenic property of bone marrow mesenchymal stem cells in nanofibrous vascular grafts, Proceedings of the National Academy of Sciences, 104 (2007) 11915.

[76] T. Okano, A. Kikuchi, Y. Sakurai, Y. Takei, N. Ogata, Temperature-responsive poly(N-isopropylacrylamide) as a modulator for alteration of hydrophilic/hydrophobic surface properties to control activation/inactivation of platelets, J Control Release, 36 (1995) 125-133.

[77] T. Okano, T. Aoyagi, K. Kataoka, K. Abe, Y. Sakurai, M. Shimada, I. Shinohara, Hydrophilic-hydrophobic microdomain surfaces having an ability to suppress platelet aggregation and their in vitro antithrombogenicity, J Biomed Mater Res, 20 (1986) 919-927.

[78] K.S. Brockman, B.F.L. Lai, J.N. Kizhakkedathu, J.P. Santerre, Hemocompatibility of Degrading Polymeric Biomaterials: Degradable Polar Hydrophobic Ionic Polyurethane versus Poly(lactic-co-glycolic) Acid, Biomacromolecules, 18 (2017) 2296-2305.

[79] M. Uchida, A. Ito, K.S. Furukawa, K. Nakamura, Y. Onimura, A. Oyane, T. Ushida, T. Yamane, T. Tamaki, T. Tateishi, Reduced platelet adhesion to titanium metal coated with apatite, albumin–apatite composite or laminin–apatite composite, Biomaterials, 26 (2005) 6924-6931.

[80] E.I. Tucker, U.M. Marzec, T.C. White, S. Hurst, S. Rugonyi, O.J.T. McCarty, D. Gailani, A. Gruber, S.R. Hanson, Prevention of vascular graft occlusion and thrombus-associated thrombin generation by inhibition of factor XI, Blood, 113 (2009) 936.

[81] A. Reheman, P. Gross, H. Yang, P. Chen, D. Allen, V. Leytin, J. Freedman, H. Ni, Vitronectin stabilizes thrombi and vessel occlusion but

plays a dual role in platelet aggregation, Journal of Thrombosis and Haemostasis, 3 (2005) 875-883.

[82] L.-J. Zhu, F. Liu, X.-M. Yu, A.-L. Gao, L.-X. Xue, Surface zwitterionization of hemocompatible poly(lactic acid) membranes for hemodiafiltration, Journal of Membrane Science, 475 (2015) 469-479.

[83] J. Li, Y. Zuo, X. Cheng, W. Yang, H. Wang, Y. Li, Preparation and characterization of nano-hydroxyapatite/polyamide 66 composite GBR membrane with asymmetric porous structure, Journal of Materials Science: Materials in Medicine, 20 (2008) 1031.

[84] Y. Ueyama, K. Ishikawa, T. Mano, T. Koyama, H. Nagatsuka, K. Suzuki, K. Ryoke, Usefulness as guided bone regeneration membrane of the alginate membrane, Biomaterials, 23 (2002).

[85] S. Nyman, J. Gottlow, T. Karring, J. Lindhe, The regenerative potential of the periodontal ligament, Journal of Clinical Periodontology, 9 (1982) 257-265.

[86] K. Gotfredsen, L. Nimb, E. Hjørting-hansen, Immediate implant placement using a biodegradable barrier, polyhydroxybutyrate-hydroxyvalerate reinforced with polyglactin 910. An experimental study in dogs, Clinical Oral Implants Research, 5 (1994) 83-91.

[87] L. Kostopoulos, T. Karring, Augmentation of the rat mandible using guided tissue regeneration, Clinical Oral Implants Research, 5 (1994) 75-82.

[88] K.-H. Kim, L. Jeong, H.-N. Park, S.-Y. Shin, W.-H. Park, S.-C. Lee, T.-I. Kim, Y.-J. Park, Y.-J. Seol, Y.-M. Lee, Y. Ku, I.-C. Rhyu, S.-B. Han, C.-P. Chung, Biological efficacy of silk fibroin nanofiber membranes for guided bone regeneration, Journal of Biotechnology, 120 (2005) 327-339.

[89] M. Masoudi Rad, S. Nouri Khorasani, L. Ghasemi-Mobarakeh, M.P. Prabhakaran, M.R. Foroughi, M. Kharaziha, N. Saadatkish, S. Ramakrishna, Fabrication and characterization of two-layered nanofibrous membrane for guided bone and tissue regeneration application, Materials Science and Engineering: C, 80 (2017) 75-87.

[90] J. Wang, L. Wang, Z. Zhou, H. Lai, P. Xu, L. Liao, J. Wei, Biodegradable Polymer Membranes Applied in Guided Bone/Tissue Regeneration: A Review, Polymers-Basel, 8 (2016).

[91] H.D. Barber, J. Lignelli, B.M. Smith, B.K. Bartee, Using a Dense PTFE Membrane Without Primary Closure to Achieve Bone and Tissue Regeneration, Journal of Oral and Maxillofacial Surgery, 65 (2007) 748-752.

[92] Y. Amano, M. Ota, K. Sekiguchi, Y. Shibukawa, S. Yamada, Evaluation of a poly-l-lactic acid membrane and membrane fixing pin for guided tissue regeneration on bone defects in dogs, Oral Surg Oral Med Oral Pathol Oral Radiol Endod, 97 (2004).

[93] H. Maeda, T. Kasuga, L.L. Hench, Preparation of poly(l-lactic acid)-polysiloxane-calcium carbonate hybrid membranes for guided bone regeneration, Biomaterials, 27 (2006) 1216-1222.

[94] S.J. Lee, Y.J. Park, S.N. Park, Y.M. Lee, Y.J. Seol, Y. Ku, C.P. Chung, Molded porous poly (L-lactide) membranes for guided bone regeneration with enhanced effects by controlled growth factor release, J Biomed Mater Res, 55 (2001).

[95] T.-S. Jang, E.-J. Lee, J.-H. Jo, J.-M. Jeon, M.-Y. Kim, H.-E. Kim, Y.-H. Koh, Fibrous membrane of nano-hybrid poly-L-lactic acid/silica xerogel for guided bone regeneration, Journal of Biomedical Materials Research Part B: Applied Biomaterials, 100B (2012) 321-330.

[96] X. Song, F. Ling, L. Ma, C. Yang, X. Chen, Electrospun hydroxyapatite grafted poly(l-lactide)/poly(lactic-co-glycolic acid) nanofibers for guided bone regeneration membrane, Composites Science and Technology, 79 (2013) 8-14.

[97] H. Maeda, T. Kasuga, Control of silicon species released from poly(lactic acid)-polysiloxane hybrid membranes, J Biomed Mater Res A, 85A (2008) 742-746.

[98] T. Wakita, A. Obata, G. Poologasundarampillai, J.R. Jones, T. Kasuga, Preparation of electrospun siloxane-poly(lactic acid)-vaterite hybrid fibrous membranes for guided bone regeneration, Composites Science and Technology, 70 (2010) 1889-1893.

[99] C. Xianmiao, L. Yubao, Z. Yi, Z. Li, L. Jidong, W. Huanan, Properties and in vitro biological evaluation of nano-hydroxyapatite/chitosan membranes for bone guided regeneration, Materials Science and Engineering: C, 29 (2009) 29-35.

[100] A.L.B. Pinheiro, M.E. Martinez Gerbi, F. de Assis Limeira, E.A. Carneiro Ponzi, A.M.C. Marques, C.M. Carvalho, R. de Carneiro Santos, P.C. Oliveira, M. Nóia, L.M.P. Ramalho, Bone repair following bone grafting hydroxyapatite guided bone regeneration and infra-red laser photobiomodulation: a histological study in a rodent model, Lasers in Medical Science, 24 (2009) 234-240.

[101] I.-G. Kang, C.-I. Park, Y.-J. Seong, H. Lee, H.-E. Kim, C.-M. Han, Bioactive and mechanically stable hydroxyapatite patterning for rapid

endothelialization of artificial vascular graft, Materials Science and Engineering: C, 106 (2020) 110287.

[102] K.L. Spiller, G. Vunjak-Novakovic, Clinical translation of controlled protein delivery systems for tissue engineering, Drug Delivery and Translational Research, 5 (2015) 101-115.

[103] Z.S. Haidar, R.C. Hamdy, M. Tabrizian, Delivery of recombinant bone morphogenetic proteins for bone regeneration and repair. Part A: Current challenges in BMP delivery, Biotechnology Letters, 31 (2009) 1817.

[104] R.J. Miron, N. Saulacic, D. Buser, T. Iizuka, A. Sculean, Osteoblast proliferation and differentiation on a barrier membrane in combination with BMP2 and TGFβ1, Clinical Oral Investigations, 17 (2013) 981-988.

[105] R.E. Jung, R. Glauser, P. Schärer, C.H.F. Hämmerle, H.F. Sailer, F.E. Weber, Effect of rhBMP-2 on guided bone regeneration in humans, Clinical Oral Implants Research, 14 (2003) 556-568.

[106] J.-H. Shim, M.-C. Yoon, C.-M. Jeong, J. Jang, S.-I. Jeong, D.-W. Cho, J.-B. Huh, Efficacy of rhBMP-2 loaded PCL/PLGA/β-TCP guided bone regeneration membrane fabricated by 3D printing technology for reconstruction of calvaria defects in rabbit, Biomedical Materials, 9

(2014) 065006.

[107] Y.-M. Lee, S.-H. Nam, Y.-J. Seol, T.-I. Kim, S.-J. Lee, Y. Ku, I.-C. Rhyu, C.-P. Chung, S.-B. Han, S.-M. Choi, Enhanced Bone Augmentation by Controlled Release of Recombinant Human Bone Morphogenetic Protein-2 from Bioabsorbable Membranes, Journal of Periodontology, 74 (2003) 865-872.

[108] K.M. Woo, J. Seo, R. Zhang, P.X. Ma, Suppression of apoptosis by enhanced protein adsorption on polymer/hydroxyapatite composite scaffolds, Biomaterials, 28 (2007) 2622-2630.

[109] H. Autefage, F. Briand-Mésange, S. Cazalbou, C. Drouet, D. Fourmy, S. Gonçalvès, J.-P. Salles, C. Combes, P. Swider, C. Rey, Adsorption and release of BMP-2 on nanocrystalline apatite-coated and uncoated hydroxyapatite/β-tricalcium phosphate porous ceramics, Journal of Biomedical Materials Research Part B: Applied Biomaterials, 91B (2009) 706-715.

[110] Y. Fujishiro, H. Yabuki, K. Kawamura, T. Sato, A. Okuwaki, Preparation of needle-like hydroxyapatite by homogeneous precipitation under hydrothermal conditions, Journal of Chemical Technology and Biotechnology, 57 (1993) 349-353.

[111] S. Ban, S. Maruno, Hydrothermal–electrochemical deposition of hydroxyapatite, J Biomed Mater Res, 42 (1998) 387-395.

[112] M. Wang, W. Bonfield, Chemically coupled hydroxyapatite–polyethylene composites: structure and properties, Biomaterials, 22 (2001) 1311-1320.

[113] M.-H. Ho, L.-T. Hou, C.-Y. Tu, H.-J. Hsieh, J.-Y. Lai, W.-J. Chen, D.-M. Wang, Promotion of Cell Affinity of Porous PLLA Scaffolds by Immobilization of RGD Peptides via Plasma Treatment, Macromolecular Bioscience, 6 (2006) 90-98.

[114] E.-H. Song, Y.-J. Seong, C. Park, I.-G. Kang, H.-E. Kim, S.-H. Jeong, Use of thioglycerol on porous polyurethane as an effective theranostic capping agent for bone tissue engineering, Journal of Biomaterials Applications, 33 (2018) 955-966.

[115] E. Röhner, P. Hoff, T. Gaber, A. Lang, P. Vörös, F. Buttgereit, C. Perka, C. Windisch, G. Matziolis, Cytokine Expression in Human Osteoblasts After Antiseptic Treatment: A Comparative Study Between Polyhexanide and Chlorhexidine, Journal of Investigative Surgery, 28 (2015) 1-7.

[116] J. Yang, Y. Wan, C. Tu, Q. Cai, J. Bei, S. Wang, Enhancing the cell

affinity of macroporous poly(L-lactide) cell scaffold by a convenient surface modification method, Polym Int, 52 (2003) 1892-1899.

[117] P.T. Sudheesh Kumar, S. Hashimi, S. Saifzadeh, S. Ivanovski, C. Vaquette, Additively manufactured biphasic construct loaded with BMP-2 for vertical bone regeneration: A pilot study in rabbit, Materials Science and Engineering: C, 92 (2018) 554-564.

[118] D.-W. Lee, Y.-P. Yun, K. Park, S.E. Kim, Gentamicin and bone morphogenic protein-2 (BMP-2)-delivering heparinized-titanium implant with enhanced antibacterial activity and osteointegration, Bone, 50 (2012) 974-982.

[119] J. Fang, P. Li, X. Lu, L. Fang, X. Lü, F. Ren, A strong, tough, and osteoconductive hydroxyapatite mineralized polyacrylamide/dextran hydrogel for bone tissue regeneration, Acta Biomater, 88 (2019) 503-513.

[120] I.-G. Kang, C.-I. Park, H. Lee, H.-E. Kim, S.-M. Lee, Hydroxyapatite Microspheres as an Additive to Enhance Radiopacity, Biocompatibility, and Osteoconductivity of Poly(methyl methacrylate) Bone Cement, Materials, 11 (2018).

[121] W. Xie, F. Song, R. Wang, S. Sun, M. Li, Z. Fan, B. Liu, Q. Zhang, J. Wang, Mechanically Robust 3D Graphene–Hydroxyapatite Hybrid

Bioscaffolds with Enhanced Osteoconductive and Biocompatible Performance, Crystals, 8 (2018).

[122] J.A. Kim, H.-s. Yun, Y.-A. Choi, J.-E. Kim, S.-Y. Choi, T.-G. Kwon, Y.K. Kim, T.-Y. Kwon, M.A. Bae, N.J. Kim, Y.C. Bae, H.-I. Shin, E.K. Park, Magnesium phosphate ceramics incorporating a novel indene compound promote osteoblast differentiation in vitro and bone regeneration in vivo, Biomaterials, 157 (2018) 51-61.

초록 (Abstract)

다양한 생체 기능과 기계적 안정성을 갖는 하이드록시아파타이트의 패터닝

서울대학교
재료공학부
강 인 구

인체 내부 뼈의 구성요소 중 하나인 하이드록시아파타이트(HA)는 조직 재생 분야에서 널리 사용되는 유망한 재료로 알려져 있다. 많은 경우에, HA는 기존 조직과의 결합력에 영향을 미치는 생체적합성을 증진시키기 위해 금속 임플란트 표면에 코팅 적용된다. 그러나, 특유의 취성으로 인해, HA는 복잡한 모양의 금속 임플란트나 유연한 고분자 표면에 적용되는데는 어려움이 있다. 바로 이점에서, 마이크로패터닝이 취성이 있는 HA를 표면에 적용하는 대안이 될 수 있다. 포토리소그래피를 이용해 제작한 HA 마이크로패턴은 본 연구진의 새로운 패턴 트랜스퍼링(Pattern transferring) 기술을 이용해 고분자 표면에 도입되었다. 이러한 방법을 이용해, 취성이 강한 HA를 기계적 안정성을 갖는 동시에 증진된 생체적합성을 부

여하면서 유연한 바이오 고분자 표면에 적용하는 것이 가능하다.

첫번째 연구에서, 본 연구진은 직선형의 HA 패턴을 실리콘 웨이퍼 상에 제작하고 이후 그 패턴을 튜브 형태의 인공 혈관으로 사용되는 폴리-L-락틱액시드(PLLA) 필름에 트랜스퍼하였다. 생체활성을 갖는 HA 패턴은 생체내 활성이 적은 고분자 인공 혈관에 생체적합성을 부여하게 된다. 고유의 바늘 형태의 구조를 갖는 HA 패턴이 PLLA 모재에 성공적으로 트랜스퍼되어 박혀있는 것을 확인하였다. HA 패턴화된 PLLA 필름은 HA가 코팅된 PLLA 필름에 비해 우수한 기계적 안정성을 갖는 것을 굽힘, 인장, 그리고 생체 모방 순환 조건 실험으로 알 수 있었다. 따라서 일련의 실험을 통해 튜브 형태의 인공 혈관으로 적용하는데 적합함을 확인하였다. 추가적으로, HA 패턴이 혈관내피세포의 패턴을 따른 증식과 이동을 촉진함으로써 신속한 혈관내피세포화(endothelialization)을 유도하였다. HA 패턴화된 PLLA의 혈액안정성은 표면에 부착된 상대적으로 적은 양의 혈소판을 통해 알 수 있었다. 전반적으로, HA 패턴화된 PLLA는 아무 처리가 되지않은 PLLA에 비해 훌륭한 기계적 안정성뿐 아니라, 증진된 생체적합성과 혈액안정성까지 보여주었다.

두번째 연구에서는, PLLA 골형성유도막(GBR 멤브레인)에 적용된 HA 패턴에 제2형 재조합인간골형성단백질(rhBMP-2)를 담지하는 새로운 방법을 개발하였다. PLLA 멤브레인에 성공적으로 만들어진 HA 패턴을 트랜스퍼하였고 기계적 자극을 줬을때도 고정되고 안정적인 형상을 보여줌을 확인했다. 단백질이 PLLA에 비해 HA 패턴 위와 아래에 명확하게 부착되었고, HA 아래에 담지된 경우에서 7일에 걸쳐 서서히 방출되는 것도 확인하였다. 담지된 rhBMP-2의 양은 HA아래 담지된 샘플(u/HAP)에서 가장 많았고, 이는 반구형 구조를 갖는 HA 패턴의 넓은 표면적 때문으로 보였다. 세포 형상과 증식 결과들은 PLLA 멤브레인에 HA가 미치는 생체적인 효과를 증명해준다. 전조골 세포의 분화(Osteoblastic differentiation) 결과는 14일 동안의 ALP 활성도의 눈에 띄는 증가를 통해 u/HAP에서의 rhBMP-2의 많은 방출량을 입증했다. 동물 실험 결과는 골재생을 유도하는 HA의 영향과 u/HAP에서 많은 양의 rhBMP-2가 방출됨에 따라 연장된 골치유 효과를 보여주었다.

결과적으로, 생체 활성을 갖는 HA 패턴이 만들어지고 PLLA 표면에 트랜스퍼되어 성공적으로 생체적합성을 부여하고 추가적인 약물 담지 기능을 부가하였다. 이와 같은 독특한 패터닝과

트랜스퍼링 기술을 통해, 취성을 갖는 생체재료를 유연한 고분자 멤브레인에 적용가능할 것으로 보이고, 이와 같은 구조를 다양한 조직공학 분야에 적용할 수 있을 것으로 기대된다.

주요어: 하이드록시아파타이트, 폴리-L-락틱액시드, 마이크로패터닝, 패턴트랜스퍼링, 인공혈관, 혈관내피세포화, 골형성유도막, 골재생, 제2형 재조합인간골형성단백질, 약물 전달

학번: 2015-20875

감사의 글(Acknowledgement)

6년이라는 긴 시간을 거쳐서 결국 때가 왔습니다. 2014년 가을, 교수님을 찾아 뵙기 위해 처음 학교에 발을 들이던 순간이 기억납니다. 낙엽을 밟으며 부푼 마음으로 33동을 찾아 헤매던 그때는 알지 못했지요. 복잡한 건물 구조에 얼마나 헤매게 될지, 어떤 사람들을 만나게 될지, 오리주물럭 맛이 어떨지, 앞으로 어떤 일들이 펼쳐질지 까지 말이죠. 그 모든 어려움들, 그 모든 즐거움들, 그 모든 순간들. 고스란히 추억으로 안고 이제 졸업하려 합니다. 졸업을 앞두고 돌이켜보니 남은 건 e-beam도 HA도 wafer도 아닌 사람들인 것 같아서, 굳이 이런 닭살 돋는 끄적거림을 논문 끝에 덧붙여 봅니다.

사랑하는 우리 가족에게 먼저 감사의 말을 남깁니다. 아버지, 어머니. 6년의 대학원 생활 동안, 방황하는 모습도, 지쳐있는 모습도, 가끔가다 자랑스러운 모습도 보셨겠지요. 두분 다 그리 다정한 타입들은 아니셨지만, 그래도 그 모든 시간을 함께해 주셔서 고맙습니다. 힘들어하는 아들보다는 스스로 묵묵히 제 갈 길을 가는 아들의 모습을 보여드리고 싶었습니다. 이미 눈치 채셨 듯 별 재능 없는 아들입니다만, 그래도 박사라 불릴 수 있게 된 건 묵묵히 매일 새벽 쌓아 올리신 아버지와 어머니의 기도 덕분입니다. 누나. 지구 상에서 나와 가장 유전적으로 닮은 생물. 누나가 이 세상에 존재하는 것만으로도 나에게 큰 힘이 돼. 오래오래 건강해. 매형. 누나를 데려가줘서 정말 고맙습니다. 이 은혜 잊지 않을게요. 잔잔했던 우리 집을 더 빛내 줘서 고맙습니다.

지도 교수님이신 김현이 교수님. 6년 동안 지도해 주셔서 정말 감사드립니다. 아무것도 모르고 졸업을 앞둔 햇병아리 학부생을 박사로 만들어주신 교수님의 은혜를 영원히 잊지 못할 것 같습니다. 교수님께서는 늘 스스로 생각할 수 있는 힘을 길러 주셨습니다. 졸업해서 어딜 가더라도 그 힘이 큰 원동력이 될 것 같습니다. 6년 동안 바보같이 굴었던 적도 많을 텐데, 단 한번도 성내지 않으시고 늘 인자하게 웃으시며 주셨던 그 도움의 말씀들을 잊지 못할 것 같습니다. 교수님께서 보여주셨던 모습을 닮아 멋진 어른이 되겠습니다. 더불어 앞으로도 교수님께 부끄럽지 않은 제자가 되도록 주어진 자리에서 노력하겠습니다.

바쁘신 와중에도 제 박사과정 학위논문을 심사 및 지도해주신 안철희 교수님, 남기태 교수님, 한철민 교수님, 정현도 교수님께도 감사의 말씀을 드립니다. 부족한 연구에 관심을 가져주시고, 그에 대한 아낌없는 조언을 해주신 덕에 무사히 학위 논문을 완성할 수 있었습니다. 짧은 지면을 빌어 다시 한번 감사의 말씀을 드립니다.

긴 세월 동안 함께해준 BMA 식구들에게도 감사의 인사를 남깁니다. 제 첫번째 논문의 교신 저자이자, 연구실 생활에 많은 도움을 주신 이성미 박사님. 아껴주시고 관심 가져 주신데 비해 늘 실망만 드리진 않았나 걱정됩니다. 연구뿐만 아니라 앞으로의 생활에 대해서도 해주신 조언들, 잊지 않고 새기면서 살겠습니다. 더불어 도환이가 훌륭한 어른이 되길 응원하겠습니다. 한철민 교수님. 논문 지도에 열정을 쏟아 주시고 실험에도 아낌없이 해주신 조언 잊지 않겠습니다. 교수님의 시크함 속에서 따스함을 느꼈던 건, 제 착각

은 아니었겠지요. 학위 논문 지도에 큰 관심을 가져주시고 힘써 주신 정현도 교수님, 연구실 생활 초반 함께 해주시고 이후에도 여러 조언을 아끼지 않으셨던 장태식 교수님께도 감사의 말씀을 드립니다. 더불어 여러 가지 연구를 함께 하며 많은 도움을 주셨던 안민경 박사님께도 감사드립니다. 또한, 연합 미팅을 통해 귀중한 조언을 아끼지 않으셨던 고영학 교수님과 실험에 많은 도움을 주신 고려대 학생 여러분에게도 깊은 감사의 말씀을 드립니다.

힘든 연구실 생활 속에서도 늘 웃음을 잃지 않으시고 따뜻하게 대해 주신 민호형, 제 연구의 기본적인 아이디어를 주시고 졸업 후에도 계속해서 도움주신 새미누나. 연구실 생활에 즐거움을 더해 주셨던 성원이형. 졸업 후에도 조언과 관심을 아끼지 않으셨던 설하누나. 제 사수이자 여러 도움을 주셨던 재욱이형. 늘 아낌없이 사랑해주신 병석이형. 스스럼없이 친하게 대해 주셨던 다영누나. 좋은 친구이자 형이 되어준 권위적인 척하는 권위 없는 현이형. 엉뚱한 모습 속에 친절함을 숨기고 계셨던 호용이형. 연구실에 귀여움을 더해 주었던 첸커형. 따뜻한 조언과 실험적인 도움, 어느 것 하나 아끼지 않았던 윤정누나. 멋진 선배이자 좋은 친구가 되어줬던 광희형. 훌륭한 본보기가 되어주어 늘 닮고 싶던 천일이형. 모두 감사한 분들 뿐 입니다.

은호, 경일이, 석우 내 친구들. 나랑 같은 날에 태어난 은호. 돌이켜보면 네 덕에 새로운 환경에 적응하기 훨씬 수월 했어. 어떨 때는 든든한 형 같고 어떨 때는 귀여운 동생 같았던 네가 참 힘이 됐어. 고맙고 앞으로도 잘 부탁해. 내가 정말 좋아하는 캐릭터의 경일이. 너의 말 하나하나가 나의 웃음 포인트를 건드려 버렸지.

힘들 때도 웃을 때도 너와 함께할 수 있어서 영광이었어. 앞으로도 날 웃겨줘. 무엇이든 꽂힌 것에 진심인 석우. 힘든 순간 함께해줘서 너무 고맙고 덕분에 잘 견딜 수 있었어. 앞으로도 그 진중한 모습 잃지 말아줘.

나와 함께해준 최후의 생존자들, 진영형, 민규, 창하, 수형. 모두 고맙습니다. 진영이형. 형 앞에서는 늘 내 본 모습이 나와요. 그게 좋은 점도 있고 꼴보기 싫은 점도 있었겠지만 모두 감내해줘서 진심으로 고마워요. 늘 꼭 안고 싶어지는 형의 모습을 잊지 못할 것 같아요♥. 나의 친구 민규. 함께해서 즐거웠다. 네 덕분에 조금이라도 더 나은 선배가 될 수 있었던 것 같아 고맙다. 그런데 민규야 늘 조심하고, 알지? 나의 스승님 창하. 친절하게 와인을 알려주던 네 모습도 씽씽이를 타며 즐거워하던 엉뚱한 네 모습도 모두 잊지 못할 거야. 든든한 수형 대장. 나랑 말이 참 잘 통하는 친구를 연구실에서 찾게 될 줄은 몰랐어. 식물도 물고기도 각자 잘 키우도록 하자.

끝으로 재미나던 훈련소 시절 발견한 좋은 시 한 수 남기며 이만 말을 줄이겠습니다. 지금 내가 생각하는 모든 사람들과 지금 나를 생각하는 모든 사람들에게 감사의 말을 전합니다.

시간이 빼앗은 해年들은 내 것이 아니다.
다가올 해들도 내 것이 아니다.
순간은 내 것이다. 순간을 깊이 생각한다면,
해와 영원을 만든 분은 내 것이다.

안드레아스 그리피우스 「시간을 바라보다」